Cell Reports

Article

RNF8-mediated regulation of Akt promotes lung cancer cell survival and resistance to DNA damage

Graphical abstract

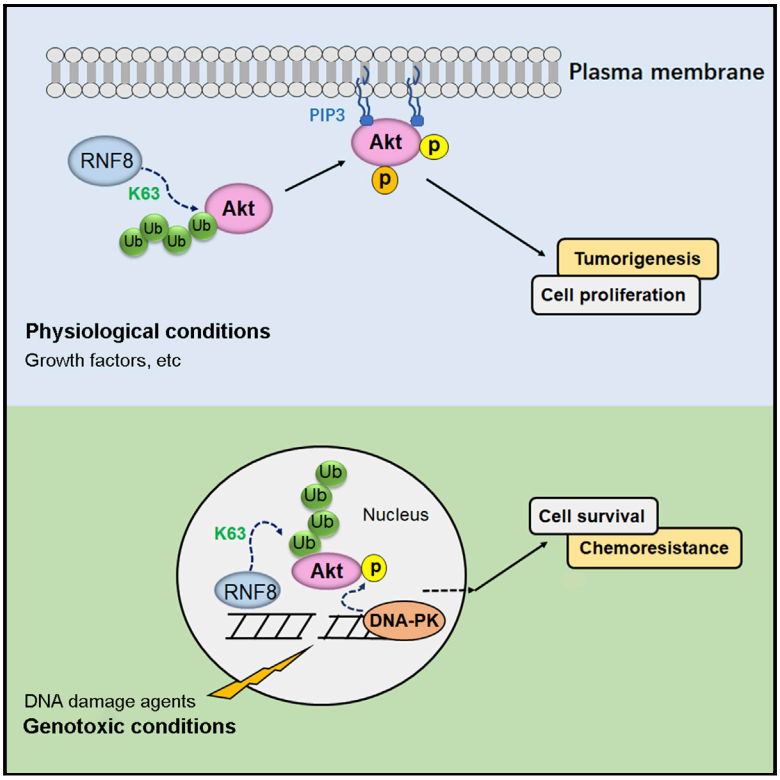

Highlights

- RNF8 promotes lung cancer progression by regulating Akt activity
- RNF8 ubiquitinates and activates Akt upon DNA damage
- RNF8-mediated Akt activation promotes chemoresistance in lung cancer

Authors

Yongjie Xu, Yumeng Hu, Tao Xu, ..., Duo Zheng, Li Li, Genze Shao

Correspondence

lily@bjmu.edu.cn (L.L.), gzshao@bjmu.edu.cn (G.S.)

In brief

Xu et al. show that E3 ligase RNF8 is overexpressed in lung cancer and regulates the activation of Akt by K63-linked ubiquitination under physiological and genotoxic conditions, leading to lung cancer cell survival and resistance to DNA damage.

Xu et al., 2021, Cell Reports *37*, 109854
October 19, 2021
https://doi.org/10.1016/j.celrep.2021.109854

CellPress

Cell Reports

CellPress
OPEN ACCESS

Article

RNF8-mediated regulation of Akt promotes lung cancer cell survival and resistance to DNA damage

Yongjie Xu,[1,9] Yumeng Hu,[1,9] Tao Xu,[2] Kaowen Yan,[3] Ting Zhang,[1] Qin Li,[1] Fen Chang,[1] Xueyuan Guo,[1] Jingyu Peng,[4] Mo Li,[5] Min Zhao,[6] Hongying Zhen,[1] Luzheng Xu,[7] Duo Zheng,[8] Li Li,[1,*] and Genze Shao[1,10,*]

[1]Department of Cell Biology, School of Basic Medical Sciences, Peking University Health Science Center, Beijing 100191, China
[2]The Affiliated Hospital of Qingdao University, Qingdao 266021, China
[3]State Key Laboratory of Membrane Biology, Institute of Zoology, Chinese Academy of Sciences, Beijing 100101, China
[4]State Key Laboratory of Membrane Biology, Ministry of Education Key Laboratory of Cell Proliferation and Differentiation, School of Life Sciences, Peking University, Beijing 100871, China
[5]Department of Obstetrics and Gynecology, Peking University Third Hospital, Beijing 100191, China
[6]Department of Oncology, Hebei Chest Hospital, Research Center of Hebei Lung Cancer Prevention and Treatment, Shijiazhuang, Hebei 050041, China
[7]Medical and Health Analysis Center, School of Basic Medical Sciences, Peking University Health Science Center, Beijing 100191, China
[8]Department of Cell Biology and Genetics, Shenzhen University School of Medicine, Shenzhen 518055, China
[9]These authors contributed equally
[10]Lead contact
*Correspondence: lily@bjmu.edu.cn (L.L.), gzshao@bjmu.edu.cn (G.S.)
https://doi.org/10.1016/j.celrep.2021.109854

SUMMARY

Despite the tremendous success of targeted and conventional therapies for lung cancer, therapeutic resistance is a common and major clinical challenge. RNF8 is a ubiquitin E3 ligase that plays essential roles in the DNA damage response; however, its role in the pathogenesis of lung cancer is unclear. Here, we report that RNF8 is overexpressed in lung cancer and positively correlates with the expression of p-Akt and poor survival of patients with non-small-cell lung cancer. In addition, we identify RNF8 as the E3 ligase for regulating the activation of Akt by K63-linked ubiquitination under physiological and genotoxic conditions, which leads to lung cancer cell proliferation and resistance to chemotherapy. Together, our study suggests that RNF8 could be a very promising target in precision medicine for lung cancer.

INTRODUCTION

Lung cancer is the leading cause of cancer mortality worldwide (Ferlay et al., 2015). Chemotherapy and radiation therapy are conventional therapies for the treatment of lung cancer; however, therapeutic resistance is a major problem (Chen et al., 2014; Gotwals et al., 2017; Holohan et al., 2013; Rotow and Bivona, 2017). Among the known mechanisms, the phosphoinositide 3-kinase (PI3K)/Akt pathway is a commonly activated signaling pathway involved in therapeutic resistance (Gadgeel and Wozniak, 2013; Liu et al., 2009).

Activation of Akt by extracellular stimuli, such as diverse growth factors (GFs), occurs in a PI3K-dependent manner. Phosphorylation of threonine 308 (T308) in the activation loop and serine 473 (S473) in the C-terminal activation domain results in full activation of Akt (Alessi et al., 1996; Calleja et al., 2007; Vanhaesebroeck et al., 2010). GFs facilitate Akt membrane recruitment and activation by inducing K63-linked ubiquitination of Akt, and distinct E3 ligases are used by different GFs (Chan et al., 2012; Yang et al., 2009). Overactivation of Akt mediates multiple pathways that favor tumorigenesis and drug resistance (Altomare and Testa, 2005; Hennessy et al., 2005; Larue and Bellacosa, 2005; Shaw and Cantley, 2006).

Apart from GFs, increasing lines of evidence suggest that various genotoxic stresses (especially DNA damage) could also activate Akt and support the important role of Akt in post-chemotherapy survival and chemoresistance of cancer cells (Brognard et al., 2001; Park et al., 2006; Yu et al., 2008). Unlike GFs, DNA-damage-induced Akt activation seems to associate with Akt pS473 that most likely occurs at the nucleus (Boehme et al., 2008; Fraser et al., 2011). However, the mechanism of Akt activation, the identity of E3 ligase involved, and whether K63-linked ubiquitination is generally induced and serves as a common mechanism for Akt activation in response to DNA damage remain unclear.

RNF8 is a RING finger E3 ligase involved in DNA damage repair (Huen et al., 2007; Kolas et al., 2007; Mailand et al., 2007). At the sites of DNA double-strand breaks (DSBs), RNF8 cooperates with Ubc13 to attach K63-linked ubiquitin moieties to L3MBTL2 and histone H1. This creates an environment for recruiting RNF168, another E3 ligase that polyubiquitylates H2A-type histones on sites flanking DSBs (Nowsheen et al., 2018;

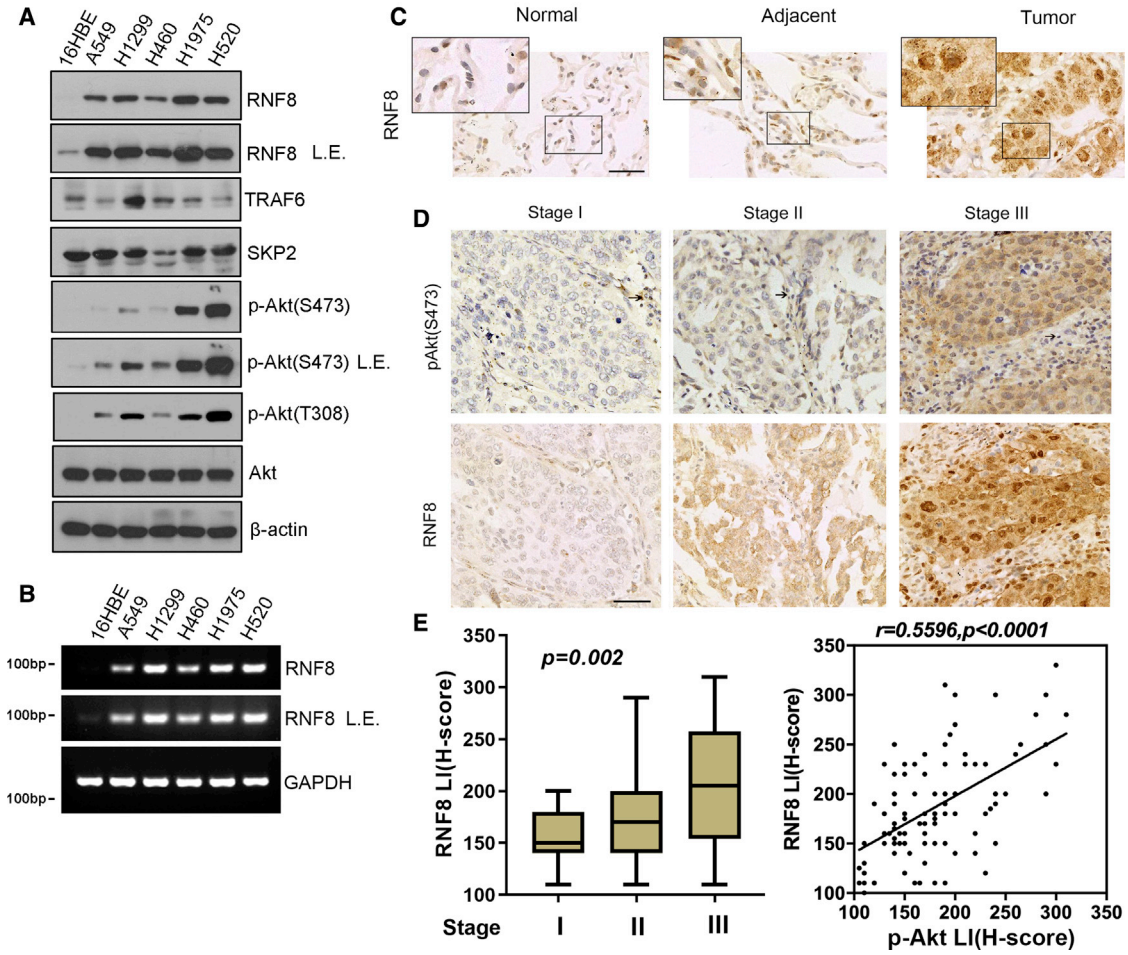

Figure 1. RNF8 is overexpressed and positively correlated with Akt phosphorylation in lung cancer

(A) RNF8 is aberrantly expressed in human lung cancer cell lines, with concomitant activation of Akt. L.E., long exposure.

(B) The mRNA levels of RNF8 are preferentially upregulated in lung cancer cell lines. Glyceraldehyde-3-phosphate dehydrogenase (GAPDH) was used as a loading control.

(C) IHC staining of RNF8 in normal lung, NSCLC, and the corresponding paired adjacent tissues. A representative image of each type of tissues is shown. Scale bar, 50 μm.

(D) Association between RNF8 expression and p-Akt(S473) was evaluated by IHC in 120 cases of lung cancer tissues within different clinicopathological TNM stages. Representative images are shown. Scale bar, 50 μm. The black arrows indicate the stromal cells and/or tumor-infiltrating lymphocytes.

(E) Statistical analysis of RNF8 expressions in lung tumors as in (D) (left); scatterplot analysis shows the correlation between the expression of RNF8 and that of p-Akt(S473) using the Pearson correlation coefficient analysis (n = 120) (right). r = 0.5596, p < 0.0001. LI, labeling index.

See also Figure S1.

Thorslund et al., 2015). Polyubiquitination of histones leads to the recruitment of other repair proteins including 53BP1 and BRCA1 to DSBs (Kolas et al., 2007; Mailand et al., 2007; Nowsheen et al., 2018). In addition to K63-linked ubiquitination, RNF8 also mediates K48-linked ubiquitination and degradation of JMJD2A upon DNA damage, facilitating recruitment of 53BP1 to DSBs (Mallette et al., 2012). Based on its role in DNA damage repair, RNF8 has long been considered a genome guardian. However, our previous work and others (Kuang et al., 2016; Lee et al., 2016) have shown that RNF8 promotes epithelial-mesenchymal transition (EMT) in breast cancer cells, suggesting the potential role of RNF8 in tumorigenesis. In addition, RNF8 overexpression was reported to activate PI3K/Akt signaling in lung cancer cells, but the detailed mechanism was not defined (Kuang et al., 2020).

Here, we show that RNF8 directly regulates Akt under physiological and genotoxic conditions. Overexpression of RNF8 is positively correlated with Akt activation and increased chemoresistance, as well as poor prognosis of lung cancer.

RESULTS

RNF8 is overexpressed and positively correlated with Akt phosphorylation in lung cancer

To explore the role of RNF8 in lung cancer, we first examined its expression in normal lung epithelial cells (16HBE) and several

lung cancer cell lines (A549, H1299, H460, H1975, and H520) by western blotting and reverse-transcriptase PCR (RT-PCR). As shown in Figures 1A and 1B, both the protein and mRNA levels of RNF8 in human lung cancer cell lines were significantly higher than those in normal 16HBE cells. To confirm this finding, we examined RNF8 expression in fresh non-small cell lung cancer (NSCLC) specimens by western blotting. As shown in Figure S1A, the expression levels of the RNF8 protein in lung cancer tissues (5/6, 83.33%) were higher than those in the paired adjacent noncancerous lung tissues. Furthermore, we evaluated RNF8 expression in 45 pairs of NSCLC tissues and the corresponding adjacent tissues, as well as in 10 normal tissues by immunohistochemistry (IHC). The immunostaining pattern was divided into low (−/+), middle (++), and high (+++) according to the score based on total staining intensity and proportion of positive cells. As shown in Figure 1C and Table S1, of the 45 paired cases examined, 12/45 (26.7%) of the lung cancer samples and only 2/45 (4.4%) of the adjacent tissues exhibited overexpression of RNF8 (+++). Interestingly, positive RNF8 staining was seen only in the nucleus in normal lung tissues and the adjacent noncancerous tissues; whereas in lung cancer tissues, it was seen in both the cytoplasm and nucleus of the cells. Next, we analyzed the association between RNF8 expression and the tumor node metastasis (TNM) stage in 120 lung cancer tissue samples. A statistical analysis showed that the expression of RNF8 was much higher in stage III cases than that in other stages, suggesting a positive relationship between RNF8 protein expression and the NSCLC TNM stage (Figures 1D and 1E). In addition, by mining data from the Oncomine database, we found that RNF8 is commonly overexpressed in different types of lung cancer, especially in squamous cell lung carcinoma (Figure S1B). Taken together, these results suggest that RNF8 might play an important role in the pathogenesis of lung cancer.

To investigate the underlying mechanism of RNF8 in the carcinogenesis of lung cancer, we examined the expression of RNF8 and activity of Akt in normal and lung cancer tissues because many E3 ligases are associated with Akt activation (Chan et al., 2012; Yang et al., 2009). As shown, phosphorylation of Akt was positively correlated with the level of RNF8 in both lung cancer cell lines and tissues (Figures 1A, 1D, 1E, and S1A). These results suggest that RNF8 might play a role in regulating the activity of Akt.

RNF8 is required for K63-linked ubiquitination of Akt

To gain an insight into the mechanism by which RNF8 regulates Akt, we first examined the interaction between RNF8 and Akt by coimmunoprecipitation (coIP). Ectopic RNF8 was detected in the Akt immunoprecipitates (Figure 2A). Akt could also coIP with endogenous RNF8 (Figure 2B). A glutathione S-transferase (GST) pull-down assay revealed that RNF8 interacts mainly with Akt1 and, to a lesser extent, Akt3 but not with Akt2 (Figures 2C and S2A).

Because RNF8 is an E3 ligase, we attempted to investigate whether it could ubiquitinate Akt. An *in vivo* ubiquitination assay was performed using endogenous Akt immunoprecipitation or nickel-nitrilotriacetic acid (Ni-NTA) pull-down under denaturing conditions. The results revealed that Akt ubiquitination was dramatically increased by the overexpression of HA-RNF8WT but not HA-RNF8ΔR, a RNF8 mutant lacking the RING domain despite its intact binding to Akt (Figures 2D, 2E, and S2B). These results suggest that the E3 ligase activity of RNF8 is critical for mediating Akt ubiquitination. Consistent with its role in promoting Akt ubiquitination, RNF8 depletion significantly inhibited Akt ubiquitination (Figure 2F). More importantly, decreased ubiquitination of endogenous Akt was also detected in RNF8-depleted A549 cells (Figure 2G). Collectively, these results indicate that RNF8 is required for Akt ubiquitination, and Akt could be a substrate of RNF8. To confirm this hypothesis, an *in vitro* ubiquitination assay was performed. As shown in Figure 2H, RNF8 readily induced Akt ubiquitination in collaboration with Ubc13. These data reveal that RNF8 is a direct E3 ligase for Akt ubiquitination.

RNF8 was previously reported to be capable of catalyzing the conjugation of both K48 and K63-linked ubiquitin chains by interacting with two different E2 ubiquitin-conjugating enzymes, namely, UbcH8 or Ubc13 (Lok et al., 2012). To determine the type of Akt ubiquitin chain modified by RNF8, an *in vivo* ubiquitination assay was performed with different ubiquitin mutants, in which the lysine residues within ubiquitin were mutated to arginine to disturb the ubiquitin chain formation at that site. As shown, RNF8-mediated ubiquitination of Akt was significantly decreased in cells transfected with K63R but not with K48R (Figure 2I). A consistent result was obtained with K63-only and K48-only ubiquitin constructs (Figure S2C). In addition, the RNF8 mutant (I405A), which is defective in binding UbcH8 and is unable to catalyze the formation of K48-linked ubiquitin chains, retains the ability to induce Akt ubiquitination (Figure S2D). Taken together, these data indicate that RNF8 is an E3 ligase for the K63-linked ubiquitination of Akt.

RNF8 deficiency inhibits tumor cell growth by regulating Akt phosphorylation and activation *in vivo*

It has been shown that K63-linked ubiquitination is required for Akt recruitment to the plasma membrane, where Akt could be subsequently phosphorylated by PDK1 and mTORC2 at the sites T308 and/or S473 for full activation (Chan et al., 2012; Yang et al., 2009). Based on this information, we reasoned that RNF8 might also play a role in regulating Akt activity. As expected, phosphorylation of Akt was increased when HA-RNF8WT was ectopically expressed but not enzymatically inactive HA-RNF8ΔR (Figure 2E). Consistently, the phosphorylation of Akt was dramatically decreased in two RNF8-KO A549 cell lines, in which the RNF8 gene was targeted by two individual single-guide RNAs (sgRNAs) (Figure 3A). In addition, we found that the phosphorylation of Akt was lower in RNF8-null mouse embryonic fibroblasts (MEFs) (*Rnf8*$^{-/-}$) than in wild-type (*WT*) MEFs (*Rnf8*$^{+/+}$), and the phosphorylation of Akt in *Rnf8*$^{-/-}$ MEFs was rescued by the restoration of RNF8WT but not the ΔR mutant (Figures 3B and 3C). These data indicate that RNF8 regulates Akt phosphorylation through its E3 ligase activity. It is noteworthy that the levels of TRAF6 and SKP2, two known E3 ligases that have been reported to regulate Akt activity, did not show any change in RNF8-depleted MEFs or A549 cells (Figures 3A and 3B), which suggests that the alteration of p-Akt might not correlate with TRAF6 or SKP2 in our experimental system.

Next, we investigated the role of RNF8-mediated ubiquitination in the activation of Akt. Mutation of K8 and K14 to arginine

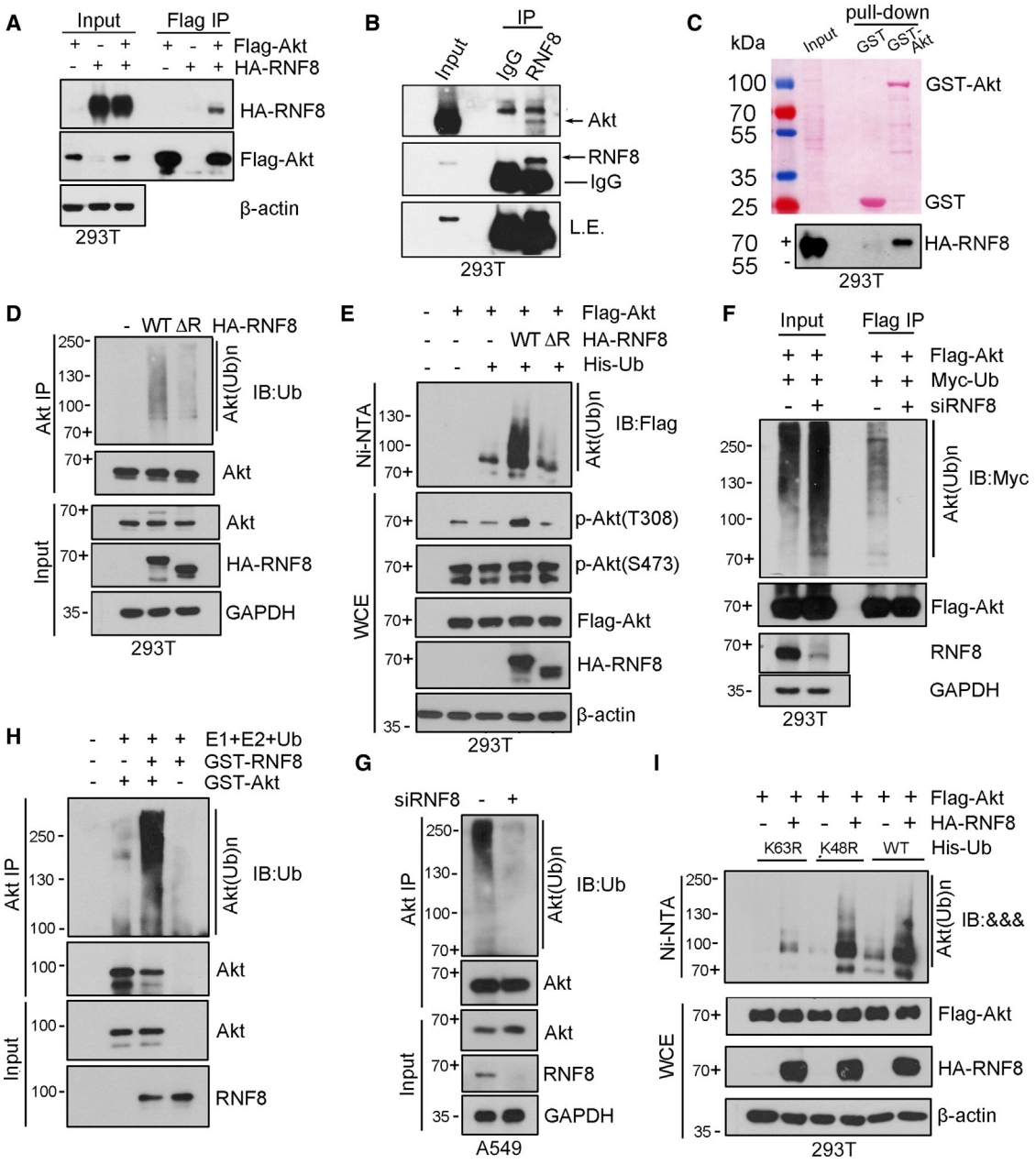

Figure 2. RNF8 is required for K63-linked ubiquitination of Akt

(A) Ectopic HA-RNF8 interacts with FLAG-Akt in 293T cells.

(B) Endogenous RNF8 interacts with endogenous Akt in 293T cells.

(C) Akt directly binds to RNF8 *in vitro*. GST or GST-Akt was incubated with the lysates from 293T cells expressing HA-RNF8. The bound proteins were pulled down by glutathione-agarose and analyzed by Ponceau staining (top) or immunoblotting (IB) with anti-hemagglutinin (HA) antibodies (bottom).

(D and E) Akt ubiquitination is increased upon overexpression of RNF8WT but not the ΔR mutant. 293T cells were transfected with HA-RNF8 WT or ΔR mutant, and the cell lysates were subjected to immunoprecipitation using anti-Akt antibodies (D) or Ni-NTA pull-down under denaturing conditions (E), followed by IB with the indicated antibodies.

(F and G) Akt ubiquitination is decreased upon RNF8 depletion. 293T cells were cotransfected with the indicated plasmids or siRNAs, and FLAG-Akt was immunoprecipitated and analyzed by IB (F); A549 cells were transfected with control or RNF8 siRNA, and endogenous Akt was immunoprecipitated and analyzed for ubiquitination (G).

(H) *In vitro* ubiquitination assay. GST-Akt was incubated with ATP, E1, and E2 (Ubc13/Uev1) along with or without purified GST-RNF8. The reaction mixtures were subjected to immunoprecipitation using anti-Akt antibodies, followed by IB analysis.

(I) RNF8 modifies Akt by K63-linked ubiquitination. 293T cells were cotransfected with the indicated plasmids, and the cell lysates were assayed for *in vivo* ubiquitination.

See also Figure S2.

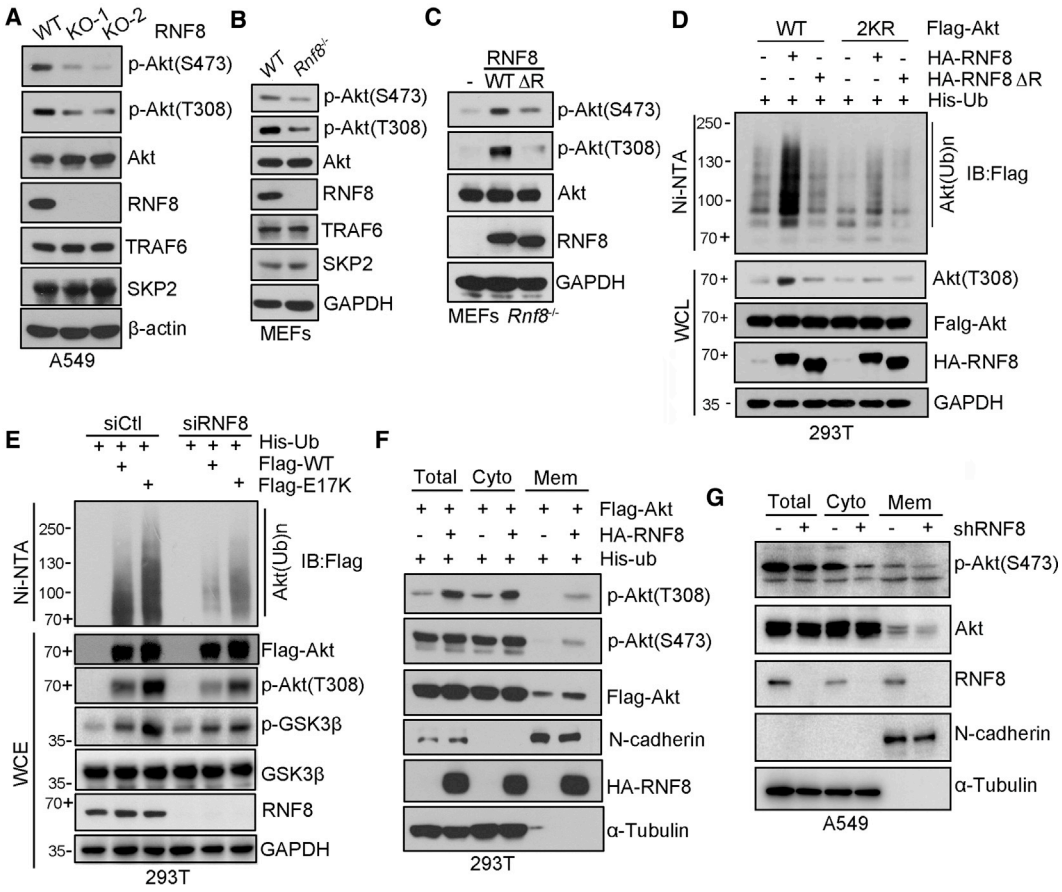

(legend on next page)

within Akt (Akt2KR mutant) was reported to disrupt its K63-linked ubiquitination (Yang et al., 2009). As shown in Figure 3D, forced expression of HA-RNF8 enhanced the ubiquitination and phosphorylation of Akt in cells transfected with FLAG-AktWT but not FLAG-Akt2KR. This result suggests that the activation of Akt induced by RNF8 overexpression depends on its ubiquitination. To confirm this hypothesis, we used FLAG-AktE17K and assessed the effects of RNF8 on its ubiquitination and activation. E17K is a common mutant of Akt identified in a variety of human cancers (Bleeker et al., 2008; Kim et al., 2008; Yang et al., 2009). E17K is constitutively activated, and increased ubiquitination is thought to contribute to its hyperactivation. As shown in Figure 3E, the ubiquitination and phosphorylation of E17K were reduced in RNF8-depleted cells. These data suggest that RNF8 might be partially involved in the hyperactivation of E17K, probably by promoting its ubiquitination.

K63-linked ubiquitination regulates Akt membrane recruitment and phosphorylation. To examine the influence of RNF8 on the membrane localization of Akt, we performed membrane fractionation to assess membrane Akt. As shown, overexpression of RNF8 increased Akt membrane distribution in 293T cells, coinciding with an increase in the phosphorylation of Akt (Figure 3F), whereas depletion of RNF8 reduced Akt membrane localization in A549 cells, concomitant with a reduction in Akt phosphorylation (Figure 3G). These results indicate that RNF8 regulates Akt activity by promoting its K63-linked ubiquitination and membrane recruitment.

Akt is frequently hyperactivated in human lung cancer and is involved in lung tumorigenesis (Balsara et al., 2004; Xu et al., 2010). Based on its role in regulating Akt, we investigated whether RNF8 could play an oncogenic role in lung cancer development. As shown, the viability of RNF8 knockout (KO) cells was significantly decreased, consistent with the reduced phosphorylation of Akt in these cells compared with WT cells. Importantly, these phenotypes caused by RNF8 depletion were rescued by the re-expression of AktE17K or RNF8WT but not RNF8ΔR (Figures 3H, S3A, and S3B). The effect of RNF8 KO on apoptosis was also observed. As shown in Figure 3I, the percentage of apoptotic cells was higher in A549-RNF8 KO cells when compared with that of WT cells, and the increased apoptosis rate could be partially compensated by the restoration of AktE17K. These results suggest that RNF8 could promote lung cancer cell survival by regulating the activity of Akt.

To further confirm the role of RNF8 in lung carcinogenesis, we assessed the consequences of RNF8 depletion on tumor growth *in vivo*. A549 stable cell lines expressing control or RNF8 short hairpin RNA (shRNA) (shRNF8-1 or -2) were subcutaneously injected into non-obese diabetic (NOD)/severe combined immunodeficiency (SCID) mice, and tumor growth was monitored. Strikingly, tumors arising from shRNF8 cells grew significantly slower than those initiated by the control shRNA cells (Figure S3C). Similar results were observed in RNF8 KO A549 cells, and importantly, the decrease in tumor growth of KO cells was partially rescued by overexpression of AktE17K (Figure 3J). IHC staining of the proliferation marker Ki-67 showed that the percentage of positive cells is about 93% in xenografts expressing RNF8-WT, whereas it is only 28% in xenografts with RNF8-KO and is dramatically increased to 75% in xenografts rescued with AktE17K (RNF8 KO+AktE17K) (Figure S3D). Together, these results demonstrated that RNF8 deficiency inhibits tumor cell proliferation by inhibiting ubiquitination and activation of Akt *in vivo*.

RNF8 promotes Akt activation in response to DNA damage

Although activation of Akt in response to DNA damage has long been recognized (Tan and Hallahan, 2003; Toulany et al., 2008; Toulany et al., 2012), the underlying details of Akt activation are largely unknown. Given its function in the DNA repair pathway and Akt ubiquitination, we attempted to investigate whether RNF8 could play a role in the activation of Akt upon DNA damage. We treated *WT* and *Rnf8*$^{-/-}$ MEFs with either

Figure 3. RNF8 deficiency inhibits tumor cell growth by regulating Akt phosphorylation and activation *in vivo*

(A) Akt phosphorylation is reduced in RNF8 KO cells. Cell lysates from A549 WT, RNF8 KO-1, and RNF8 KO-2 cells were subjected to IB analysis, using the indicated antibodies.

(B and C) Akt phosphorylation is reduced in *Rnf8*$^{-/-}$ MEFs and restored by re-expression of RNF8WT but not the ΔR mutant. (B) *Rnf8*$^{+/+}$ and *Rnf8*$^{-/-}$ MEFs were harvested for IB analysis. (C) *Rnf8*$^{-/-}$ MEFs infected with lentiviruses expressing mock, human RNF8 (hRNF8), or human RNF8ΔR (hRNF8ΔR) were harvested, and the cell lysates were analyzed by IB using the indicated antibodies.

(D) FLAG-Akt2KR is defective in ubiquitination and activation upon RNF8 overexpression. 293T cells were cotransfected with the indicated plasmids for 48 h. Lysates were used for Ni-NTA pull-down followed by IB analysis.

(E) FLAG-AktE17K ubiquitination and phosphorylation are inhibited by RNF8 depletion. 293T cells were cotransfected with the indicated siRNAs and plasmids. Lysates were used for Ni-NTA pull-down followed by IB analysis.

(F) Overexpression of RNF8 promotes Akt membrane translocation. 293T cells were transfected with the indicated plasmids and fractionated. The membrane (Mem) and cytosolic (Cyto) protein extracts were subjected to IB analysis.

(G) The membrane translocation of Akt is reduced in RNF8 depleted cells. The membrane (Mem) and cytosolic (Cyto) fractions extracted from A549 cells transfected with control or RNF8 shRNA were analyzed by IB.

(H) Decreased survival of cells with RNF8 depletion is rescued by reintroduction of AktE17K or RNF8WT but not RNF8ΔR. Cell viability was assayed in RNF8 WT and KO A549 cells infected with control or lentiviruses expressing the indicated proteins. Data are normalized to day 1. Results are presented as mean values ± SD (n = 3). ***p < 0.001 versus KO, Student's t test. n.s, no significance.

(I) Apoptosis induced by RNF8 depletion is rescued by re-expression of AktE17K. RNF8 WT and KO A549 cells infected with control or AktE17K were harvested for apoptosis analysis. Results are presented as mean values ± SD (n = 3). *p < 0.05 versus KO, Student's t test.

(J) Tumor growth inhibited by RNF8 knockout is partially restored by re-expression of AktE17K. RNF8 WT and KO A549 cells infected with lentiviruses expressing control or AktE17K were subcutaneously injected into nude mice, and tumorigenesis was monitored. Left, xenograft tumors formed in each group of mice. Right, tumor growth curves of the A549 xenograft tumors. Results are presented as mean values ± SD. ***p < 0.001 versus KO, Student's t test.

See also Figure S3.

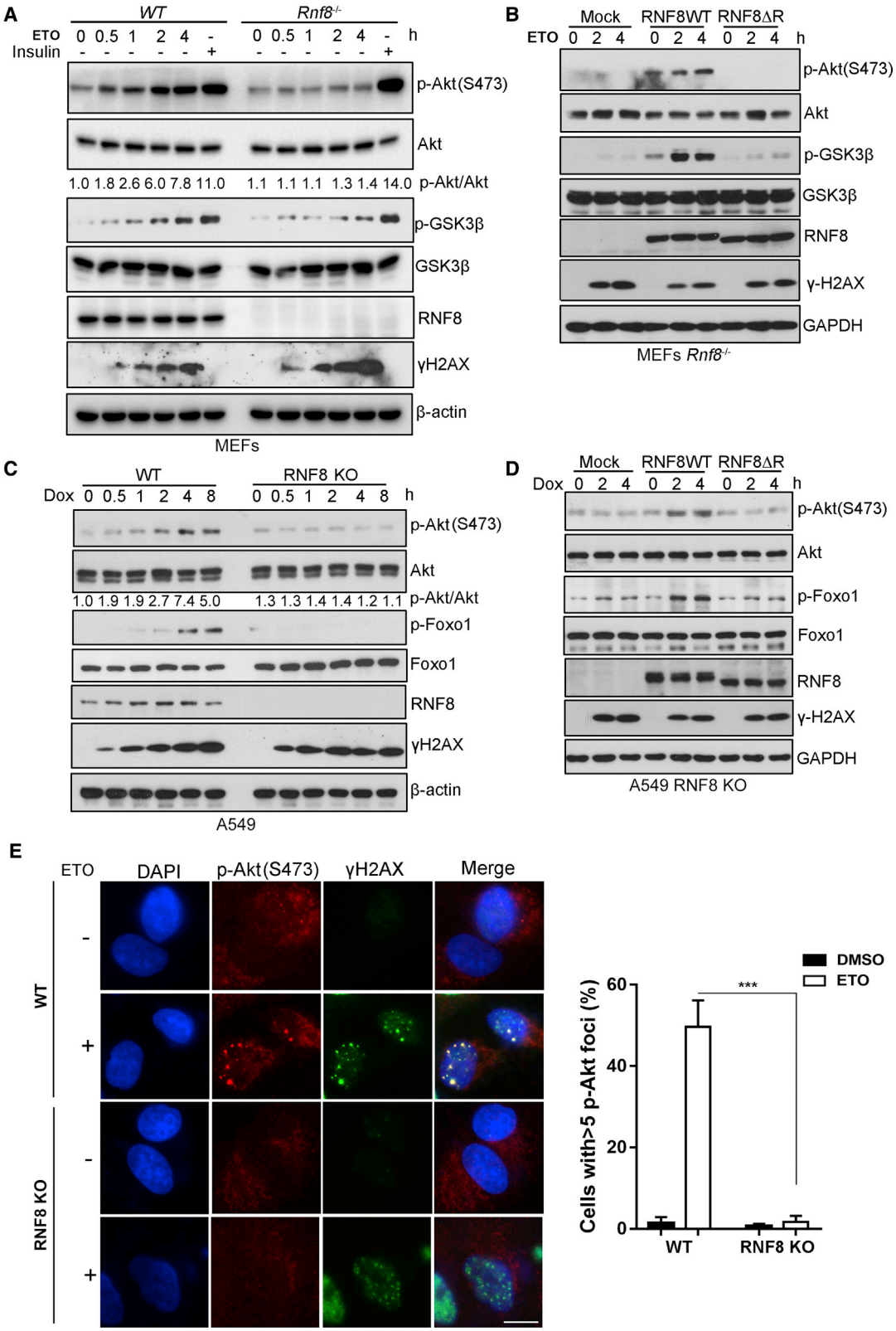

(legend on next page)

etoposide (ETO) or insulin and examined the phosphorylation and activation of Akt. ETO treatment induced DNA damage in both *WT* and *Rnf8*$^{-/-}$ MEFs, as indicated by increased γH2AX. Strikingly, ETO treatment induced Akt activation in *WT* MEFs, whereas this effect was abolished in *Rnf8*$^{-/-}$ MEFs (Figures 4A and S4A). In contrast, Akt activation in response to insulin was barely affected in *Rnf8*$^{-/-}$ MEFs when compared with that in *WT* (Figure 4A). Importantly, the defective phosphorylation of Akt in *Rnf8*$^{-/-}$ MEFs could be rescued by re-expression of RNF8WT but not the RNF8ΔR mutant (Figure 4B). These results indicate that RNF8 plays an essential role in DNA-damage-induced Akt activation, probably through a mechanism dependent on its E3 ligase activity. To further confirm these results, RNF8 KO A549 cells were treated with doxorubicin (Dox) or ETO, and phosphorylation of Akt, as well as its downstream effector Foxo-1, was assessed. As shown, Akt phosphorylation was induced in WT A549 cells upon Dox and ETO treatment but was completely abolished in RNF8 KO cells (Figures 4C and S4B–S4D), and it was further rescued by reintroduction of RNF8WT but not the RNF8ΔR mutant (Figure 4D). Moreover, consistent with the previous report (Bozulic et al., 2008), we also observed obvious p-Akt (S473) foci in A549 cells following treatment with ETO. However, this ETO-induced p-Akt (S473) foci formation was entirely abolished in RNF8 KO cells (Figure 4E). Together, these results indicate that RNF8 is required for DNA-damage-induced activation of Akt.

RNF8 is responsible for the DNA-damage-induced ubiquitination of Akt

Previous studies have shown that K63-linked ubiquitination is required for Akt activation. Based on this information, we asked whether DNA-damage-induced activation of Akt is associated with its ubiquitination. As shown, the level of Akt ubiquitination, as well as its phosphorylation, was increased in cells treated with Dox or ETO, and Akt was modified mainly through K63-linked ubiquitin chains (Figure 5A), a ubiquitin species primarily observed in the DNA damage repair pathway (Schwertman et al., 2016). Moreover, although ubiquitination and phosphorylation of Akt were enhanced following treatment with Dox in both MEFs and A549 cells with WT RNF8, they were almost abolished in RNF8-depleted cells (Figures 5B and 5C). Consistently, immunoprecipitation using either Akt or RNF8 antibodies showed that the association of RNF8 with Akt was notably enhanced upon DNA damage (Figures 5C and 5D). These data suggest that DNA-damage-triggered Akt ubiquitination is dependent on RNF8. Because RNF8-mediated ubiquitination is required for Akt membrane recruitment and subsequent activation under physiological conditions (Figures 3F and 3G), we attempted to investigate whether a similar mechanism for Akt activation could be used in the context of DNA damage. Cells were treated with or without Dox, followed by fractionation and subsequent Akt immunoprecipitation. Surprisingly, we found that the ubiquitination of Akt triggered by Dox mainly occurred in the nucleus but not in the cytoplasm (Figure 5E). Accordingly, DNA-damage-triggered Akt phosphorylation was mainly detected in the nuclear extract or at sites of DNA damage (Figures 4E and 5F). These results suggest that a different signaling from that of physiological conditions may be used to mediate the ubiquitination and activation of Akt in response to DNA damage.

DNA-damage-induced ubiquitination is required for Akt activation

To further investigate the role of ubiquitination in Akt activation in the context of DNA damage, we compared the levels of ubiquitination and phosphorylation of different Akt variants in response to Dox treatment. We found that the phosphorylation level of AktE17K was much higher than that of WT when cells were treated with Dox (Figure 6A). Concomitantly, a higher level of K63Ubs was detected in AktE17K (Figure 6B). These results suggest that DNA-damage-induced ubiquitination of Akt might contribute to its activation. In contrast to AktE17K, Akt2KR was found to be defective in Dox-induced K63-linked ubiquitination (Figure 6C) and displayed impaired phosphorylation following Dox treatment (Figure 6A), indicating that K63-linked ubiquitination of Akt is indispensable for its activation in DNA damage.

In order to assess the role of RNF8 in Akt activation in the context of DNA damage, we compared the phosphorylation of either FLAG-AktWT or FLAG-AktE17K in RNF8 WT and KO cells. As expected, Dox treatment could induce phosphorylation of both WT and E17K Akt in RNF8 WT cells, but this change was abolished in RNF8 KO cells (Figure 6D). These data further suggest that DNA-damage-induced activation of Akt depends on RNF8.

As reported, DNA-damage-induced synthesis of K63Ub is mainly mediated by Ubc13, an essential E2 paired with RNF8 (Wang and Elledge, 2007). Next, we further verified the importance of K63-linked ubiquitination in Akt activation under

Figure 4. RNF8 is required for activation of Akt upon DNA damage

(A) RNF8 is required for ETO-induced Akt activation. *WT* and *Rnf8*$^{-/-}$ MEFs were serum starved and treated with 50 μM ETO or with 100 nM insulin for the indicated time, and the cell lysates were analyzed by IB.

(B) The RING domain is essential for RNF8-mediated activation of Akt in response to ETO treatment. *Rnf8*$^{-/-}$ MEFs infected with mock, hRNF8, or hRNF8ΔR mutant were serum starved and treated with 50 μM ETO for the indicated time and harvested for IB analysis.

(C) RNF8 is required for Dox-induced activation of Akt. WT and RNF8 KO A549 cells were serum starved and treated with 5 μM Dox for the indicated time, and cell lysates were analyzed by IB.

(D) The RING domain is essential for RNF8-mediated activation of Akt in response to Dox treatment. RNF8 KO A549 cells were treated and analyzed as in (B) except for Dox treatment.

(E) RNF8 is required for ETO-induced p-Akt(S473) foci formation. WT and RNF8 KO A549 cells were serum starved and treated with DMSO or 50 μM ETO for 2 h and fixed for immunofluorescence analysis. Left, representative images of Akt(S473) foci formed in each group. Scale bar, 10 μm. Right, quantitative analysis of foci as shown in the Left. Results are presented as mean values ± SD. ***$p < 0.001$ using Student's t test.

See also Figure S4.

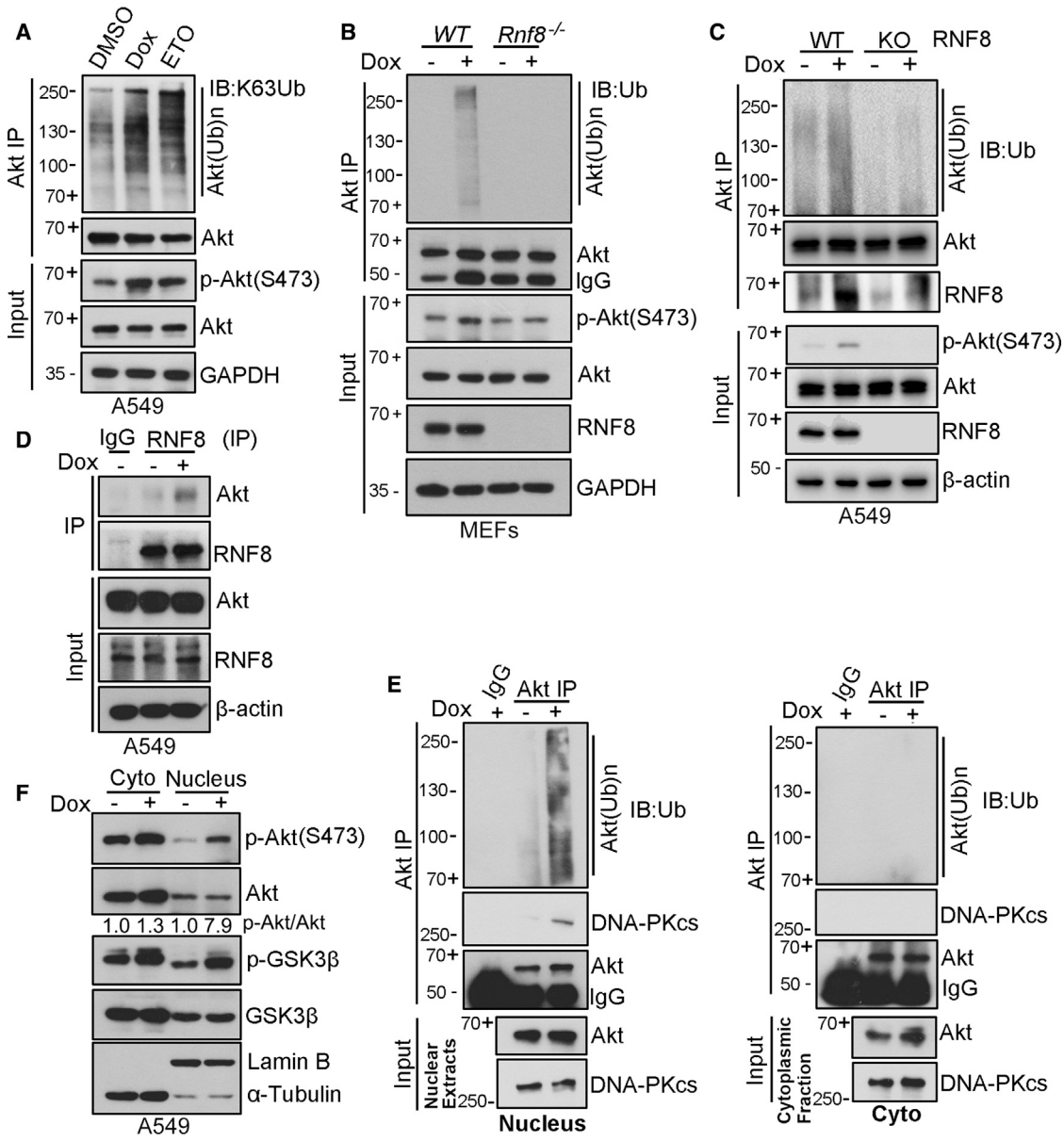

Figure 5. RNF8 is required for DNA-damage-induced ubiquitination of Akt

(A) Dox or ETO treatment induces K63-lined ubiquitination of Akt. A549 cells were serum starved and treated with 5 μM Dox or 50 μM ETO for 2 h; the cells were harvested and an immunoprecipitation assay was conducted with anti-Akt antibodies, followed by IB analysis.

(B and C) Dox-induced ubiquitination of Akt is defective in *Rnf8*$^{-/-}$ MEFs and RNF8 KO A549 cells. *WT* and *Rnf8*$^{-/-}$ MEFs (B) or WT and RNF8 KO A549 cells (C) were treated as in (A) and Akt was immunoprecipitated, followed by IB analysis.

(D) The interaction between Akt and RNF8 is increased upon Dox treatment. A549 cells were treated as in (A), and RNF8 was immunoprecipitated and analyzed by IB.

(E) Nuclear Akt is ubiquitinated and interacts with DNA-PKs in response to Dox treatment. A549 cells were treated with 5 μM Dox for 2 h and fractionated. Nuclear (left) and cytosolic (right) extracts were subjected to immunoprecipitation using immunoglobulin G (IgG) or anti-Akt antibodies, followed by IB analysis.

(F) Nuclear Akt is activated upon Dox treatment. A549 cells were treated as in (E). Nuclear and cytosolic fractions were subjected to IB analysis.

conditions of DNA damage by inhibiting Ubc13. We found that Dox-induced ubiquitination of Akt was completely inhibited in A549 cells treated with NSC697923, an inhibitor of Ubc13 (Pulvino et al., 2012; Figure 6E). Consequently, NSC697923 treatment significantly repressed the enhancement of Akt phosphorylation in response to Dox treatment (Figure 6F). A similar result was observed in A549 cells when Ubc13 was depleted by RNAi (Figure S5A). These results further support the vital role of K63-linked ubiquitination in DNA-damage-induced activation of Akt.

Next, we explored how the ubiquitination of Akt facilitates its activation. DNA-dependent protein kinase catalytic subunit (DNA-PKcs) is responsible for DNA-damage-induced activation

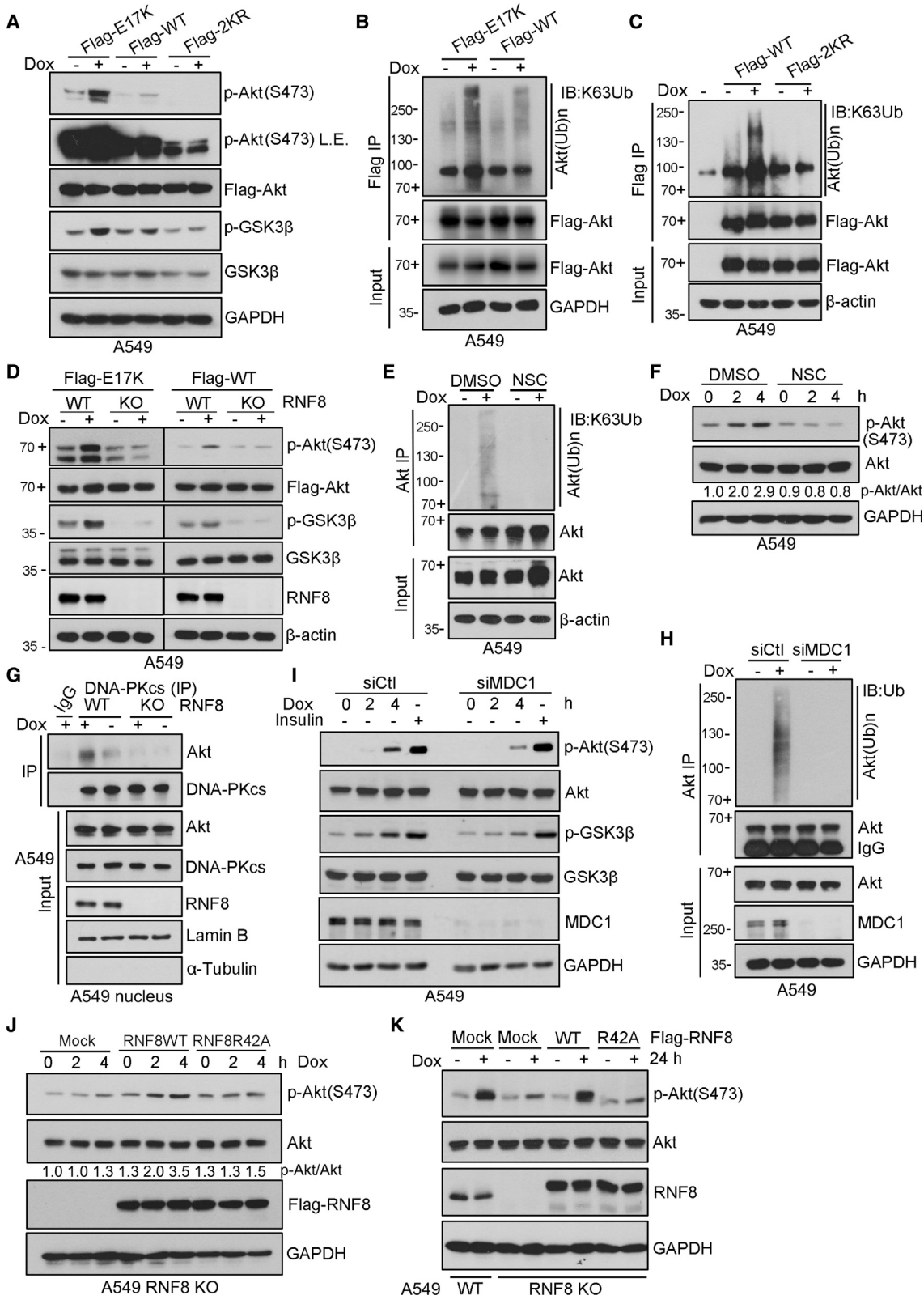

(legend on next page)

of Akt (Bozulic et al., 2008), and we confirmed that conclusion in A549 cells by using inhibitor or siRNA against DNA-PKcs (Figure S5B). To understand the precise mechanism by which the ubiquitination of Akt promotes its activation during DNA damage response (DDR), the interaction of DNA-PKcs with Akt was compared in WT and RNF8 KO cells with or without Dox treatment. The interaction of DNA-PKcs with nuclear, but not cytoplasmic Akt, was significantly enhanced upon Dox treatment in WT cells (Figures 5E and 6G), whereas this interaction was almost abrogated in RNF8 KO cells (Figure 6G). This finding suggests that Akt ubiquitination promotes its interaction with or accessibility to DNA-PKcs, which in turn could lead to Akt phosphorylation by DNA-PKcs.

As MDC1-mediated RNF8 recruitment to the DNA damage sites is a prerequisite for the execution of RNF8 function (Mailand et al., 2007; Nowsheen et al., 2018), we attempted to explore whether activation of Akt requires recruitment of RNF8 at DNA damage sites. As shown, MDC1 depletion abrogated RNF8 recruitment to the DNA damage sites (Figure S5C) and accordingly abolished the ubiquitination and activation of Akt, as well as p-Akt (S473) foci formation induced by DNA damage agents but not by insulin (Figures 6H, 6I, and S5D). Importantly, defects in Akt phosphorylation in RNF8 KO A549 cells during DDR could be rescued by re-expression of RNF8WT but not RNF8R42A (Figures 6J and 6K), which is a mutant of RNF8 that is unable to get to the DNA damage sites due to its deficiency in the recognition of MDC1 (Kolas et al., 2007), but it can still interact with Akt (Figure S5E). Together, these data imply that the recruitment of RNF8 to DNA damage sites is required for the ubiquitination and subsequent activation of Akt.

RNF8 promotes chemoresistance of lung cancer cells and predicts poor survival of patients with NSCLC

Hyperactivation of Akt is associated with chemoresistance in various cancers by inhibiting DNA-damage-induced apoptosis and promoting DNA damage repair (Brognard et al., 2001; Brown et al., 2015; Toulany et al., 2008, Toulany et al., 2012). Because RNF8 is required for Akt ubiquitination and activation upon DNA damage, we investigated the role of RNF8 in chemotherapy, which is known to induce DNA damage. As expected, the sensitivity of A549 cells to Dox was greatly enhanced when RNF8 was knocked out. However, this increase could be partially reversed by re-expression of either AktE17K or AktWT but not Akt2KR (Figure 7A). The result was validated in another NSCLC cell line, namely, H460 (Figures S6A and S6B). These results indicate that RNF8 plays an important role in promoting chemoresistance in lung cancer cells by regulating Akt activity by K63-linked ubiquitination and further suggest that overexpression of RNF8 in cancer might exacerbate patient outcomes of DSB-inducing therapy.

To further evaluate the role of RNF8 in chemoresistance *in vivo*, we explored the correlation between RNF8 levels and the response of patients to chemotherapy. IHC staining of RNF8 was performed in lung tumors from patients who received the chemotherapeutics ETO or cisplatin as the primary therapy. Compared with chemotherapeutic-responsive cases, patients who eventually developed recurrent tumors following chemotherapy exhibited a higher expression of RNF8 in their tumors. Moreover, a concomitant upregulation of Akt phosphorylation was also found in cases with high RNF8 expression (Figure 7B). These findings suggest that the RNF8-Akt axis is a pathologically relevant mechanism for chemoresistance. Because overexpression of RNF8 promotes cell proliferation and chemoresistance of lung cancer cells, we attempted to find out whether RNF8 could influence the survival of patients with NSCLC. The Kaplan-Meier PLOT (KM-PLOT) database (Győrffy et al., 2013) reveals that a higher expression of RNF8 is associated with worse overall survival (OS; $p = 0.014$) and free progression survival (FPS; $p = 0.012$) of patients with lung cancer (Figure S6C). Moreover, data from the Human Protein Atlas database also suggest that a higher expression of RNF8 is associated with poor survival in many other cancer types (Uhlen et al., 2017), such as liver and

Figure 6. DNA-damage-induced ubiquitination is required for Akt activation

(A) Dox treatment induces abnormal phosphorylation of Akt mutants. A549 cells transfected with the indicated plasmids were serum starved and treated with or without Dox for 2 h; the cell lysates were used for IB analysis.

(B) The ubiquitination of AktE17K is increased in response to Dox treatment. A549 cells transfected with FLAG-E17K or FLAG-WT of Akt were treated as in (A), and Akt WT or E17K was immunoprecipitated and analyzed for ubiquitination.

(C) Dox-induced ubiquitination is defective in cells expressing Akt2KR. A549 cells transfected with FLAG-AktWT or FLAG-Akt2KR were treated as in (A), and both types of Akt were immunoprecipitated and analyzed for ubiquitination.

(D) Dox-induced phosphorylation of FLAG-AktWT and -E17K depends on RNF8. WT and RNF8 KO A549 cells transfected with FLAG-AktWT or -E17K plasmids were serum starved and treated with or without Dox for 4 h, the cell lysates were subjected to IB analysis.

(E) Dox-induced ubiquitination of Akt is inhibited by the treatment of Ubc13 inhibitor NSC697923. Serum-starved A549 cells were pretreated with DMSO or 20 μM NSC697923 for 4 h and then treated with Dox (5 μM) for 2 h. Akt was immunoprecipitated and analyzed for ubiquitination.

(F) Dox-induced phosphorylation of Akt is inhibited by the treatment of NSC697923. A549 cells were pretreated with DMSO or 20 μM NSC697923 for 4 h and subsequently treated with 5 μM Dox for the indicated time. The cell lysates were analyzed by IB.

(G) The interaction between DNA-PKs and Akt is increased in WT but not in RNF8 KO A549 cells upon treatment with Dox. Serum-starved WT and RNF8 KO A549 cells were treated with 5 μM Dox for 2 h, and DNA-PKcs in the nuclear fractions was immunoprecipitated and analyzed.

(H) Dox-induced ubiquitination of Akt is impaired upon MDC1 depletion. A549 cells with control or MDC1 knockdown were serum starved and treated with 5 μM Dox for 4 h. Akt was immunoprecipitated and analyzed for ubiquitination.

(I) Dox-induced phosphorylation of Akt was affected in cells with MDC1 depletion. A549 cells with control or MDC1 knockdown were serum starved and treated with 5 μM Dox or with 100 nM insulin for the indicated time and harvested for IB analysis.

(J and K) The defect in the phosphorylation of Akt in RNF8 KO A549 cells upon Dox treatment was rescued by re-expression of RNF8 WT but not R42A. RNF8 KO A549 cells infected with the indicated plasmids were serum starved and treated with 5 μM Dox for the indicated time and harvested for IB analysis (J). A549 WT, A549 RNF8 KO, or A549 RNF8 KO infected with the indicated plasmids were treated with 2 μM Dox for 24 h and harvested for IB analysis (K).

See also Figure S5.

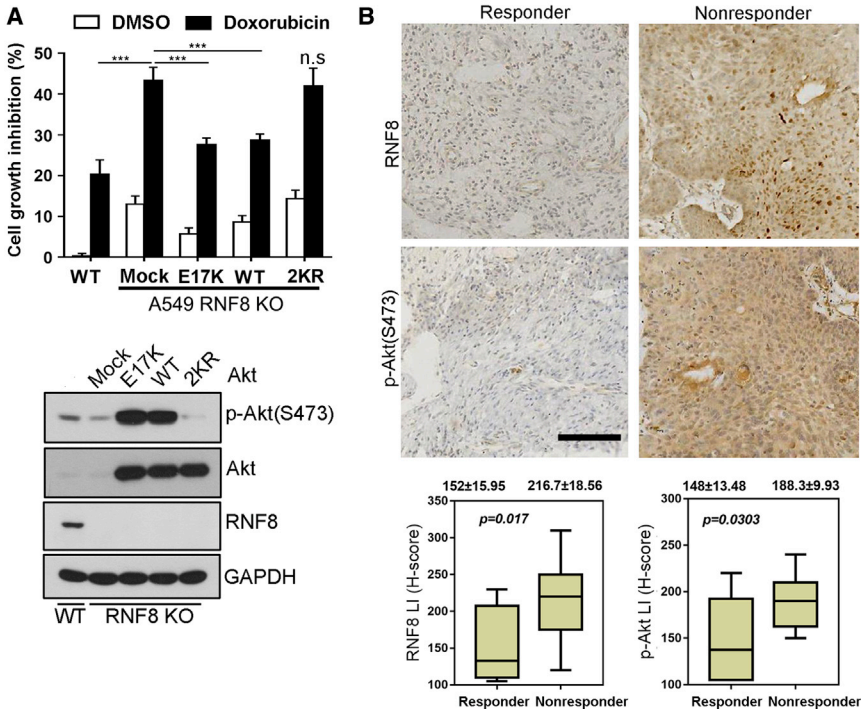

Figure 7. RNF8 promotes chemoresistance of lung cancer and predicts poor survival of patients with NSCLC

(A) The increased sensitivity to Dox in RNF8 KO A549 cells is partially reversed by re-introduction of AktWT or AktE17K but not the Akt2KR mutant. Top, cell growth inhibition assay was performed in A549 WT or RNF8 KO cells infected with the indicated plasmids in response to the treatment of Dox. Data are shown as mean values ± SD of 3 independent experiments. ***$p < 0.001$ versus KO (mock) using Student's t test. n.s, no significance. Bottom, WB confirmation of the expression of Akt and p-Akt in the A549 cell lines described above.

(B) Expression of RNF8 and p-Akt(S473) negatively correlates to the chemotherapy response in patients with lung cancer. Immunohistochemical staining (top) and quantification analyses (bottom) of RNF8 and p-Akt(S473) in tissues from patients with lung cancer with progressive or stable disease after receiving ETO or cisplatin as a primary treatment (n = 10 in each group). Scale bar, 200 μm. The results are quantified and presented as mean values ± SD.

See also Figure S6.

prostate cancer, as well as melanoma (Figure S6D). Taken together, these data suggest that RNF8 could be an important target for precision medicine or could serve as a potential predictor for cancer treatment.

DISCUSSION

A critical step for Akt activation is its ubiquitination, which usually occurs in the cytoplasm and is required for subsequent translocation to the plasma membrane where it can be phosphorylated by mTORC2/PDK1. This scenario is seen in GF-triggered activation of Akt; TRAF6 and SKP2 were reported to be the two E3 ligases involved in these processes (Chan et al., 2012; Yang et al., 2009). Here, we identify RNF8 as another E3 ligase for Akt ubiquitination and activation. Overexpression of RNF8 in lung cancer leads to hyperactivation of Akt and subsequent aberrant cancer cell proliferation and malignancy. In support of our findings, a recent study showed that Akt1 is a direct target of RNF8; however, they showed that RNF8-mediated Akt ubiquitination promotes its degradation and thus inhibits Akt/mTOR signaling upon pro-inflammatory cytokine stimulation in ulcerative colitis mice (Zhu et al., 2020). This role of RNF8 seems in contrast with our current findings showing that RNF8-mediated ubiquitination of Akt is a K63-linked, non-degradative process that facilitates Akt membrane recruitment and activation in lung cancer cells. Consistently, Kuang et al. (2020) also reported a role of RNF8 in activating Akt in lung cancer, but no detailed mechanism was provided. This discrepancy in the effects of RNF8 on Akt function suggests that RNF8-mediated regulation of Akt might be cell-context dependent. Taken together, our study underlies a role of RNF8 in promoting Akt membrane translocation and activation through K63-linked ubiquitination, further extending our understanding of the role of the RNF8-Akt axis in lung tumorigenesis and progression.

Apart from GFs, DNA damage has also been shown to activate Akt (Tan and Hallahan, 2003; Toulany et al., 2008, 2012). However, the mechanism of Akt activation during DDR and whether K63-linked ubiquitination is involved remains unclear. Here, we find that K63-linked ubiquitination is required for DNA-damage-induced Akt phosphorylation and activation, and RNF8 seems to be responsible for this ubiquitination. Unlike GFs, DNA-damage-agent-induced ubiquitination and activation of Akt mainly occurred in the nucleus. In line with our finding, a recent study from Jendrossek's lab suggests that membrane targeting or localization of Akt is associated with its effect in promoting cell growth and proliferation, whereas nuclear localization and activation are associated with resistance to irradiation (IR) (Oeck et al., 2017). In addition, they demonstrated that the E17K mutation confers cells with much more resistance to IR. In recognition of this information, we extend our study and discover that AktE17K is more liable to be ubiquitinated by RNF8 and thus more easily to be activated during DDR. Our finding provides a mechanistic interpretation for the acquisition of increased chemoresistance for E17K. Together, our data show that modification of Akt by K63Ubs seems to be a common prerequisite for its activation, highlighting the important role of K63Ubs in the regulation of Akt activity.

Although DNA-damage-triggered K63Ub modification of Akt is required for its phosphorylation by facilitating its interaction with DNA-PKcs, the precise mechanism by which K63-linked ubiquitination of Akt promotes its interaction with DNA-PKcs is unknown. So far, there is no report to prove that DNA-PKcs could

recognize K63Ub chains. One possibility is that the ubiquitination of Akt might promote its accessibility to DNA damage sites where DNA-PKcs is localized. Interestingly, phosphatidylinositol-3,4,5-trisphosphate (PIP3) and PI3K have been reported to be present (concentrated) at DNA damage foci (Kumar et al., 2010). If this finding is true, then the ubiquitination of Akt at the PH domain might promote its binding with PIP3, thus recruiting Akt in the vicinity of DSBs where it could be phosphorylated by DNA-PKcs. As such, this hypothesis could explain why PI3K is also required for DNA-damage-induced activation of Akt, as shown in previous reports (Bozulic et al., 2008; Brown et al., 2015).

The role of RNF8 in DDR has been well documented. RNF8 promotes DNA damage repair by recruiting 53BP1 and BRCA1 to the sites of DNA damage. Depletion of RNF8 results in impaired DNA repair, and Rnf8 null cells are hypersensitive to IR and DNA damage agents (Kolas et al., 2007; Li et al., 2010; Mailand et al., 2007; Zhou et al., 2013). These data suggest that RNF8 is important for genome stability and cell survival under genotoxic stresses. In this study, we discover another role of RNF8 in promoting cell survival during DDR. RNF8 ubiquitinates Akt and regulates its activity. This RNF8-dependent activation of Akt during DDR could play an essential role in preventing apoptosis of cells with excessive, unrepaired DNA damage. These two disparate functions of RNF8 might coordinate with each other to promote cell survival while ensuring genome integrity, and dysregulation of RNF8 might cause aberrant DNA repair and increased cell survival, leading to the selective survival of cells with genomic instability, which is a basis for tumorigenesis and therapeutic resistance of cancer cells.

In summary, our study suggests that RNF8 could be an important target for cancer therapy. By targeting RNF8, scientists may find out ways to overcome chemoresistance by enhancing the sensitivity of cancer cells to DNA damage. Therefore, an anticancer treatment strategy that uses targeting of RNF8 in combination with chemotherapy would be promising in the future.

STAR★METHODS

Detailed methods are provided in the online version of this paper and include the following:

- KEY RESOURCES TABLE
- RESOURCE AVAILABILITY
  - Lead contact
  - Materials availability
  - Data and code availability
- EXPERIMENTAL MODEL AND SUBJECT DETAILS
  - Cell lines
  - Mice
  - Human tissue
- METHOD DETAILS
  - RT-PCR
  - Plasmids and cloning
  - Transfection of plasmids and siRNA
  - Immunoprecipitation (IP) and immunoblotting (IB)
  - Immunofluorescence microscopy
  - *In vivo* and *in vitro* ubiquitination assay
  - Cell fractionation
  - Membrane fractionation
  - Apoptosis assay
  - *In vivo* tumorigenesis assay
  - Cell growth assay
  - Immunohistochemistry and scoring
- QUANTIFICATION AND STATISTICAL ANALYSIS

SUPPLEMENTAL INFORMATION

Supplemental information can be found online at https://doi.org/10.1016/j.celrep.2021.109854.

ACKNOWLEDGMENTS

This work was supported by the National Key Research and Development Program of China (2017YFA0503900) and the National Natural Science Foundation of China (81572711 and 81672859).

AUTHOR CONTRIBUTIONS

Y.X., L.L., and G.S. conceived and designed the experiments; Y.X., L.L., Y.H., Q.L., H.Z., D.Z., and M.L. performed the experiments; X.G. and J.P. participated in the animal study; T.X. and K.Y. contributed with clinical samples; L.X. contributed with statistical analysis; F.C. and T.Z. designed the sgRNA for RNF8; M.Z. performed IHC; Y.X., Y.H., L.L., and G.S. organized and analyzed the data and wrote the manuscript. All authors read and approved the final manuscript.

DECLARATION OF INTERESTS

The authors declare no competing interests.

Received: November 25, 2020
Revised: August 18, 2021
Accepted: September 28, 2021
Published: October 19, 2021

REFERENCES

Alessi, D.R., Andjelkovic, M., Caudwell, B., Cron, P., Morrice, N., Cohen, P., and Hemmings, B.A. (1996). Mechanism of activation of protein kinase B by insulin and IGF-1. EMBO J. *15*, 6541–6551.

Altomare, D.A., and Testa, J.R. (2005). Perturbations of the AKT signaling pathway in human cancer. Oncogene *24*, 7455–7464.

Balsara, B.R., Pei, J., Mitsuuchi, Y., Page, R., Klein-Szanto, A., Wang, H., Unger, M., and Testa, J.R. (2004). Frequent activation of AKT in non-small cell lung carcinomas and preneoplastic bronchial lesions. Carcinogenesis *25*, 2053–2059.

Bleeker, F.E., Felicioni, L., Buttitta, F., Lamba, S., Cardone, L., Rodolfo, M., Scarpa, A., Leenstra, S., Frattini, M., Barbareschi, M., et al. (2008). AKT1(E17K) in human solid tumours. Oncogene *27*, 5648–5650.

Boehme, K.A., Kulikov, R., and Blattner, C. (2008). p53 stabilization in response to DNA damage requires Akt/PKB and DNA-PK. Proc. Natl. Acad. Sci. USA *105*, 7785–7790.

Bozulic, L., Surucu, B., Hynx, D., and Hemmings, B.A. (2008). PKBalpha/Akt1 acts downstream of DNA-PK in the DNA double-strand break response and promotes survival. Mol. Cell *30*, 203–213.

Brognard, J., Clark, A.S., Ni, Y., and Dennis, P.A. (2001). Akt/protein kinase B is constitutively active in non-small cell lung cancer cells and promotes cellular survival and resistance to chemotherapy and radiation. Cancer Res. *61*, 3986–3997.

Brown, K.K., Montaser-Kouhsari, L., Beck, A.H., and Toker, A. (2015). MERIT40 Is an Akt Substrate that Promotes Resolution of DNA Damage Induced by Chemotherapy. Cell Rep. *11*, 1358–1366.

Calleja, V., Alcor, D., Laguerre, M., Park, J., Vojnovic, B., Hemmings, B.A., Downward, J., Parker, P.J., and Larijani, B. (2007). Intramolecular and intermolecular interactions of protein kinase B define its activation in vivo. PLoS Biol. *5*, e95.

Chan, C.H., Li, C.F., Yang, W.L., Gao, Y., Lee, S.W., Feng, Z., Huang, H.Y., Tsai, K.K., Flores, L.G., Shao, Y., et al. (2012). The Skp2-SCF E3 ligase regulates Akt ubiquitination, glycolysis, herceptin sensitivity, and tumorigenesis. Cell *149*, 1098–1111.

Chen, Z., Fillmore, C.M., Hammerman, P.S., Kim, C.F., and Wong, K.K. (2014). Non-small-cell lung cancers: a heterogeneous set of diseases. Nat. Rev. Cancer *14*, 535–546.

Ferlay, J., Soerjomataram, I., Dikshit, R., Eser, S., Mathers, C., Rebelo, M., Parkin, D.M., Forman, D., and Bray, F. (2015). Cancer incidence and mortality worldwide: sources, methods and major patterns in GLOBOCAN 2012. Int. J. Cancer *136*, E359–E386.

Fraser, M., Harding, S.M., Zhao, H., Coackley, C., Durocher, D., and Bristow, R.G. (2011). MRE11 promotes AKT phosphorylation in direct response to DNA double-strand breaks. Cell Cycle *10*, 2218–2232.

Gadgeel, S.M., and Wozniak, A. (2013). Preclinical rationale for PI3K/Akt/mTOR pathway inhibitors as therapy for epidermal growth factor receptor inhibitor-resistant non-small-cell lung cancer. Clin. Lung Cancer *14*, 322–332.

Gao, F., Cheng, J., Shi, T., and Yeh, E.T.H. (2006). Neddylation of a breast cancer-associated protein recruits a class III histone deacetylase that represses NFkappaB-dependent transcription. Nat Cell Biol. *8*, 1171–1177.

Gotwals, P., Cameron, S., Cipolletta, D., Cremasco, V., Crystal, A., Hewes, B., Mueller, B., Quaratino, S., Sabatos-Peyton, C., Petruzzelli, L., et al. (2017). Prospects for combining targeted and conventional cancer therapy with immunotherapy. Nat. Rev. Cancer *17*, 286–301.

Győrffy, B., Surowiak, P., Budczies, J., and Lánczky, A. (2013). Online survival analysis software to assess the prognostic value of biomarkers using transcriptomic data in non-small-cell lung cancer. PLoS One *8*, e82241.

Hennessy, B.T., Smith, D.L., Ram, P.T., Lu, Y., and Mills, G.B. (2005). Exploiting the PI3K/AKT pathway for cancer drug discovery. Nat. Rev. Drug Discov. *4*, 988–1004.

Holohan, C., Van Schaeybroeck, S., Longley, D.B., and Johnston, P.G. (2013). Cancer drug resistance: an evolving paradigm. Nat. Rev. Cancer *13*, 714–726.

Huen, M.S., Grant, R., Manke, I., Minn, K., Yu, X., Yaffe, M.B., and Chen, J. (2007). RNF8 transduces the DNA-damage signal via histone ubiquitylation and checkpoint protein assembly. Cell *131*, 901–914.

Kim, M.S., Jeong, E.G., Yoo, N.J., and Lee, S.H. (2008). Mutational analysis of oncogenic AKT E17K mutation in common solid cancers and acute leukaemias. Br. J. Cancer *98*, 1533–1535.

Kolas, N.K., Chapman, J.R., Nakada, S., Ylanko, J., Chahwan, R., Sweeney, F.D., Panier, S., Mendez, M., Wildenhain, J., Thomson, T.M., et al. (2007). Orchestration of the DNA-damage response by the RNF8 ubiquitin ligase. Science *318*, 1637–1640.

Kuang, J., Li, L., Guo, L., Su, Y., Wang, Y., Xu, Y., Wang, X., Meng, S., Lei, L., Xu, L., and Shao, G. (2016). RNF8 promotes epithelial-mesenchymal transition of breast cancer cells. J. Exp. Clin. Cancer Res. *35*, 88.

Kuang, J., Min, L., Liu, C., Chen, S., Gao, C., Ma, J., Wu, X., Li, W., Wu, L., and Zhu, L. (2020). RNF8 Promotes Epithelial-Mesenchymal Transition in Lung Cancer Cells via Stabilization of Slug. Mol. Cancer Res. *18*, 1638–1649.

Kumar, A., Fernandez-Capetillo, O., and Carrera, A.C. (2010). Nuclear phosphoinositide 3-kinase beta controls double-strand break DNA repair. Proc. Natl. Acad. Sci. USA *107*, 7491–7496.

Larue, L., and Bellacosa, A. (2005). Epithelial-mesenchymal transition in development and cancer: role of phosphatidylinositol 3′ kinase/AKT pathways. Oncogene *24*, 7443–7454.

Lee, H.J., Li, C.F., Ruan, D., Powers, S., Thompson, P.A., Frohman, M.A., and Chan, C.H. (2016). The DNA Damage Transducer RNF8 Facilitates Cancer Chemoresistance and Progression through Twist Activation. Mol. Cell *63*, 1021–1033.

Li, L., Halaby, M.J., Hakem, A., Cardoso, R., El Ghamrasni, S., Harding, S., Chan, N., Bristow, R., Sanchez, O., Durocher, D., and Hakem, R. (2010). Rnf8 deficiency impairs class switch recombination, spermatogenesis, and genomic integrity and predisposes for cancer. J. Exp. Med. *207*, 983–997.

Liu, P., Cheng, H., Roberts, T.M., and Zhao, J.J. (2009). Targeting the phosphoinositide 3-kinase pathway in cancer. Nat. Rev. Drug Discov. *8*, 627–644.

Lok, G.T., Sy, S.M., Dong, S.S., Ching, Y.P., Tsao, S.W., Thomson, T.M., and Huen, M.S. (2012). Differential regulation of RNF8-mediated Lys48- and Lys63-based poly-ubiquitylation. Nucleic Acids Res. *40*, 196–205.

Mailand, N., Bekker-Jensen, S., Faustrup, H., Melander, F., Bartek, J., Lukas, C., and Lukas, J. (2007). RNF8 ubiquitylates histones at DNA double-strand breaks and promotes assembly of repair proteins. Cell *131*, 887–900.

Mallette, F.A., Mattiroli, F., Cui, G., Young, L.C., Hendzel, M.J., Mer, G., Sixma, T.K., and Richard, S. (2012). RNF8- and RNF168-dependent degradation of KDM4A/JMJD2A triggers 53BP1 recruitment to DNA damage sites. EMBO J. *31*, 1865–1878.

Nowsheen, S., Aziz, K., Aziz, A., Deng, M., Qin, B., Luo, K., Jeganathan, K.B., Zhang, H., Liu, T., Yu, J., et al. (2018). L3MBTL2 orchestrates ubiquitin signalling by dictating the sequential recruitment of RNF8 and RNF168 after DNA damage. Nat. Cell Biol. *20*, 455–464.

Oeck, S., Al-Refae, K., Riffkin, H., Wiel, G., Handrick, R., Klein, D., Iliakis, G., and Jendrossek, V. (2017). Activating Akt1 mutations alter DNA double strand break repair and radiosensitivity. Sci. Rep. *7*, 42700.

Park, C.M., Park, M.J., Kwak, H.J., Lee, H.C., Kim, M.S., Lee, S.H., Park, I.C., Rhee, C.H., and Hong, S.I. (2006). Ionizing radiation enhances matrix metalloproteinase-2 secretion and invasion of glioma cells through Src/epidermal growth factor receptor-mediated p38/Akt and phosphatidylinositol 3-kinase/Akt signaling pathways. Cancer Res. *66*, 8511–8519.

Pulvino, M., Liang, Y., Oleksyn, D., DeRan, M., Van Pelt, E., Shapiro, J., Sanz, I., Chen, L., and Zhao, J. (2012). Inhibition of proliferation and survival of diffuse large B-cell lymphoma cells by a small-molecule inhibitor of the ubiquitin-conjugating enzyme Ubc13-Uev1A. Blood *120*, 1668–1677.

Rotow, J., and Bivona, T.G. (2017). Understanding and targeting resistance mechanisms in NSCLC. Nat. Rev. Cancer *17*, 637–658.

Schwertman, P., Bekker-Jensen, S., and Mailand, N. (2016). Regulation of DNA double-strand break repair by ubiquitin and ubiquitin-like modifiers. Nat. Rev. Mol. Cell Biol. *17*, 379–394.

Shaw, R.J., and Cantley, L.C. (2006). Ras, PI(3)K and mTOR signalling controls tumour cell growth. Nature *441*, 424–430.

Tan, J., and Hallahan, D. (2003). Growth factor-independent activation of Akt contributes to the viability of irradiated vascular endothelium. Cancer Res. *57*, S316–S317.

Thorslund, T., Ripplinger, A., Hoffmann, S., Wild, T., Uckelmann, M., Villumsen, B., Narita, T., Sixma, T.K., Choudhary, C., Bekker-Jensen, S., and Mailand, N. (2015). Histone H1 couples initiation and amplification of ubiquitin signalling after DNA damage. Nature *527*, 389–393.

Toulany, M., Kehlbach, R., Florczak, U., Sak, A., Wang, S., Chen, J., Lobrich, M., and Rodemann, H.P. (2008). Targeting of AKT1 enhances radiation toxicity of human tumor cells by inhibiting DNA-PKcs-dependent DNA double-strand break repair. Mol. Cancer Ther. *7*, 1772–1781.

Toulany, M., Lee, K.J., Fattah, K.R., Lin, Y.F., Fehrenbacher, B., Schaller, M., Chen, B.P., Chen, D.J., and Rodemann, H.P. (2012). Akt promotes post-irradiation survival of human tumor cells through initiation, progression, and termination of DNA-PKcs-dependent DNA double-strand break repair. Mol. Cancer Res. *10*, 945–957.

Uhlen, M., Zhang, C., Lee, S., Sjöstedt, E., Fagerberg, L., Bidkhori, G., Benfeitas, R., Arif, M., Liu, Z., Edfors, F., et al. (2017). A pathology atlas of the human cancer transcriptome. Science *357*, eaan2507.

Vanhaesebroeck, B., Guillermet-Guibert, J., Graupera, M., and Bilanges, B. (2010). The emerging mechanisms of isoform-specific PI3K signalling. Nat. Rev. Mol. Cell Biol. *11*, 329–341.

Wang, B., and Elledge, S.J. (2007). Ubc13/Rnf8 ubiquitin ligases control foci formation of the Rap80/Abraxas/Brca1/Brcc36 complex in response to DNA damage. Proc. Natl. Acad. Sci. USA *104*, 20759–20763.

Xu, C.X., Jin, H., Shin, J.Y., Kim, J.E., and Cho, M.H. (2010). Roles of protein kinase B/Akt in lung cancer. Front. Biosci. (Elite Ed.) *2*, 1472–1484.

Yang, W.L., Wang, J., Chan, C.H., Lee, S.W., Campos, A.D., Lamothe, B., Hur, L., Grabiner, B.C., Lin, X., Darnay, B.G., and Lin, H.K. (2009). The E3 ligase TRAF6 regulates Akt ubiquitination and activation. Science *325*, 1134–1138.

Yu, H.G., Ai, Y.W., Yu, L.L., Zhou, X.D., Liu, J., Li, J.H., Xu, X.M., Liu, S., Chen, J., Liu, F., et al. (2008). Phosphoinositide 3-kinase/Akt pathway plays an important role in chemoresistance of gastric cancer cells against etoposide and doxorubicin induced cell death. Int. J. Cancer *122*, 433–443.

Zhou, H., Mu, X., Chen, J., Liu, H., Shi, W., Xing, E., Yang, K., and Wu, G. (2013). RNAi silencing targeting RNF8 enhances radiosensitivity of a non-small cell lung cancer cell line A549. Int. J. Radiat. Biol. *89*, 708–715.

Zhu, Y., Shi, Y., Ke, X., Xuan, L., and Ma, Z. (2020). RNF8 induces autophagy and reduces inflammation by promoting AKT degradation via ubiquitination in ulcerative colitis mice. J. Biochem. *168*, 445–453.

STAR★METHODS

KEY RESOURCES TABLE

REAGENT or RESOURCE	SOURCE	IDENTIFIER
Antibodies		
Rabbit anti-Akt	Cell Signaling Technology	Cat#9272; RRID: AB_329827
Rabbit anti-phospho-Akt(Ser473)	Cell Signaling Technology	Cat#4060; RRID:AB_2315049
Rabbit anti-phospho-Akt(Thr308)	Cell Signaling Technology	Cat#13038T; RRID:AB_2629447
Rabbit anti-GSK3β	Cell Signaling Technology	Cat#9315; RRID:AB_2629447
Rabbit anti-phospho-GSK3β(S9)	Cell Signaling Technology	Cat#9336; RRID:AB_331405
Rabbit anti-Foxo1	Cell Signaling Technology	Cat#2880; RRID:AB_2106495
Rabbit anti-phospho-Foxo1(S256)	Cell Signaling Technology	Cat#9461; RRID:AB_329831
Mouse anti-Ubiquitin	Cell Signaling Technology	Cat#3936; RRID:AB_331292
Rabbit anti-K63 specific Polyubiquitin	Cell Signaling Technology	Cat#12930; RRID:AB_2798064
Rabbit anti-GAPDH	Cell Signaling Technology	Cat#5174; RRID: AB_10622025
Mouse anti-RNF8	Santa Cruz	Cat#sc-271462; RRID:AB_10648902
Rabbit anti-β-actin	ABclonal	Cat#AC026; RRID: AB_2768234
Mouse anti-Flag	Sigma	Cat#F3165; RRID:AB_259529
Mouse anti-HA	Sigma	Cat#H3663; RRID:AB_262051
Rabbit anti-MDC1	absin	Cat#abs118433; N/A
Mouse anti-N-cadherin	BD Biosciences	Cat#12674; N/A
Rabbit anti-Ubc13	abcam	Cat#ab109286; RRID:AB_10859319
Rabbit anti-TRAF6	abcam	Cat#ab33915; RRID:AB_778572
Rabbit anti-SKP2	abcam	Cat#ab183039; N/A
Rabbit anti-pChk1(S296)	abcam	Cat#ab79758; RRID:AB_2244917
Rabbit anti-pChk2(T68)	abcam	Cat#ab32148; RRID:AB_726828
Rabbit anti- JMJD2A	abcam	Cat#ab191433; N/A
Rabbit anti-Ki67	abcam	Cat#ab15580; RRID:AB_443209
Fluorescein (FITC) AffiniPure Goat Anti-Mouse IgG(H+L)	Jackson	Cat#115-095-003; N/A
Fluorescein (FITC) AffiniPure Goat Anti-Rabbit IgG(H+L)	Jackson	Cat#111-095-003; N/A
Rhodamine (TRITC) AffiniPure Goat Anti-Mouse IgG(H+L)	Jackson	Cat#115-025-146; N/A
Rhodamine (TRITC) AffiniPure Goat Anti-Rabbit IgG(H+L)	Jackson	Cat#111-025-003; N/A
Bacterial and virus strains		
DH5α Competent Cells	Biomed	Cat#BC102
BL21 (DE3) Competent Cells	Biomed	Cat#BC201
Stbl3 Competent Cells	Biomed	Cat#BC108
Biological samples		
Patient lung cancer tissue: Figure 1	National Human Genetic Resources Sharing Service Platform	2005DKA21300
Patient lung cancer tissue: Figure 7	The Affiliated Hospital of Qingdao University	N/A
Chemicals, peptides, and recombinant proteins		
Dulbecco's modified Eagle's medium (DMEM)	Macgene	Cat#CM10017
Fetal Bovine Serum (FBS)	Hyclone	Cat#SH30070.03
Penicillin-Streptomycin	Thermo Fisher Scientific	Cat#15070063

(*Continued on next page*)

Continued

REAGENT or RESOURCE	SOURCE	IDENTIFIER
Trypsin-EDTA (0.05%)	Thermo Fisher Scientific	Cat#25300062
Etoposide	Selleck Chemicals	Cat#S1125
Doxorubicin	Selleck Chemicals	Cat#S1208
NSC697923	Selleck Chemicals	Cat#S7142
NU7026	Selleck Chemicals	Cat#S2893
EGF	Peprotech	Cat#AF-100-15
IGF-1	Peprotech	Cat#100-11
Insulin	Sigma	Cat#11061-68-0
Polybrene	Sigma	Cat#TR-1003
jetPRIME	Polyplus	Cat#114-15
Protease Inhibitor Cocktail	Sigma	Cat#P8340
Phenylmethylsulfonyl Fluoride	Sigma	Cat#P7626
DNase I	Yeasen	Cat#10607ES15
Protein G-Sepharose	Biodragon	Cat#BDTL0003
Glutathione Sepharose 4B	Sigma	Cat#GE17-0756-01
Anti-Flag-M2-agarose	Sigma	Cat#A2220
Ni-NTA agarose	QIAGEN	Cat#30210
Flag-peptide	Sigma	Cat#F3290
TRIzol	Thermo Fisher Scientific	Cat#10296028
Matrigel	Corning	Cat#354234
Dihydrochloride (DAPI)	Vector Laboratories	Cat#H-1200-10
EDTA pH 9.0	ZSGB-BIO	Cat#ZLI-9079
Critical commercial assays		
Quick Start Bradford Protein Assay	Bio-Rad	Cat#5000201
Mem-PERTM Plus kit	Thermo Fisher Scientific	Cat#89842
Annexin V-PE/7-AAD Apoptosis Kit	Yeasen	Cat#40310ES20
GTVision TM Detection kit	Genetech	Cat#GK500705
AxyPrep Plasmid Midiprep Kit	Axygen	Cat#AP-MD-P
M5 HiPer First Strand cDNA Synthesis Kit	Mei5bio	Cat#MF011
GoldenStar T6 Super PCR Mix (1.1x)	TSINGKE	Cat#TSE101
GTVision^{TM}+Detection System/Mo&Rb	Gene Tech	Cat#GK600705
Deposited data		
RNF8 gene expression in subtypes of lung cancers (Figure S1B)	Oncomine	https://www.oncomine.org/index.jsp
Correlation between RNF8 mRNA expression level and patient survival in lung cancer (Figure S6C)	Kaplan-Meier Plotter	https://kmplot.com/analysis/
Correlation between RNF8 mRNA expression level and patient survival in other cancers (Figure S6D)	The Human Protein Atlas	https://www.proteinatlas.org/
Experimental models: Cell lines		
Human: HEK293T	ATCC	Cat#CRL-3216
Human: 16HBE	ATCC	Cat#CRL-2741
Human: A549	ATCC	Cat#CCL-185
Human: H1299	ATCC	Cat#CRL-5803
Human: H460	ATCC	Cat#HTB-177
Human: H520	ATCC	Cat#HTB-182
Human: H1975	Dr. Hongying Zhen, Peking University Health Science Center	N/A
Human: A549 RNF8$^{-/-}$-1	This Paper	N/A

(*Continued on next page*)

Continued

REAGENT or RESOURCE	SOURCE	IDENTIFIER
Human: A549 RNF8$^{-/-}$ −2	This Paper	N/A
Human: A549 RNF8$^{-/-}$-1+Akt	This Paper	N/A
Human: A549 RNF8$^{-/-}$-2+Akt	This Paper	N/A
Human: A549 RNF8$^{-/-}$-1+AktE17K	This Paper	N/A
Human: A549 RNF8$^{-/-}$-2+AktE17K	This Paper	N/A
Human: H460 RNF8$^{-/-}$-1	This Paper	N/A
Mouse: Mouse embryonic fibroblasts (MEFs)	Dr. Mo Li, Peking University Third Hospital	N/A
Mouse: MEFs RNF8$^{-/-}$	Dr. Mo Li, Peking University Third Hospital	N/A
Experimental models: Organisms/strains		
Mouse: BALB/c Nude	Experimental Animal Center of Peking University Health Center	N/A
Oligonucleotides		
siRNA targeting sequence: RNF8: GGACAAUUAUGGACAACAA	Thermo Fisher Scientific	https://rnaidesigner.thermofisher.com/rnaiexpress/
siRNA targeting sequence: Ubc13: UUCCAGAAGAAUACCCAAUTT	Thermo Fisher Scientific	https://rnaidesigner.thermofisher.com/rnaiexpress/
siRNA targeting sequence: DNA-PKcs: CCAGAGATTTCGGTTTGCTTGTATT	Thermo Fisher Scientific	https://rnaidesigner.thermofisher.com/rnaiexpress/
siRNA targeting sequence: MDC1: UCCAGUGAAUCCUUGAGGUTT	Thermo Fisher Scientific	https://rnaidesigner.thermofisher.com/rnaiexpress/
shRNA targeting sequence: RNF8 #1: GGACAAUUAUGGACAACAA	Thermo Fisher	https://rnaidesigner.thermofisher.com/rnaiexpress/
shRNA targeting sequence: RNF8 #2: ACATGAAGCCGTTATGAAT	GeneChem	N/A
sgRNA targeting sequence: RNF8 #1: CACCGTTCGTCACAGGAGACCGCGC	ZHANG LAB	https://zlab.bio/guide-design-resources
sgRNA targeting sequence: RNF8 #2: CACCGGAGCCCGGCTTCTTCGTCAC	ZHANG LAB	https://zlab.bio/guide-design-resources
Primers for RT-PCR: human RNF8 Forward: GGAGAAAAGGACCTGAAGCAACA	Zhu et al., 2020	N/A
Primers for RT-PCR: human RNF8 Reverse: GCTTCAAAGTCCTTCTTGCTGCG	Zhu et al., 2020	N/A
Primers for RT-PCR: human GAPDH Forward: GTCTCCTCTGACTTCAACAGCG	Zhu et al., 2020	N/A
Primers for RT-PCR: human GAPDH Reverse: ACCACCCTGTTGCTGTAGCCAA	Zhu et al., 2020	N/A
Recombinant DNA		
pcDNA3.1-HA-RNF8	This Paper	N/A
pcDNA3.1-HA-RNF8-ΔRING	This Paper	N/A
pcDNA3.1-HA-RNF8-I405A	This Paper	N/A
pcDNA3.1-Flag-RNF8	This Paper	N/A
pcDNA3.1-Flag-Akt	Dr. Hongquan Zhang, Peking University Health Science Center	N/A
pcDNA3.1-Flag-Akt-E17K	This Paper	N/A
pcDNA3.1-Flag-Akt-K8/14R	This Paper	N/A
pcDNA3.1-Myc-Ub	This Paper	N/A
pcDNA3.1-HA-Ub	This Paper	N/A
pcDNA3.1-His-Ub	This Paper	N/A
pcDNA3.1-His-Ub K63R	Dr. Jiadong Wang, Peking University Health Science Center	N/A

(*Continued on next page*)

Continued

REAGENT or RESOURCE	SOURCE	IDENTIFIER
pcDNA3.1-His-Ub K48R	Dr. Jiadong Wang, Peking University Health Science Center	N/A
pcDNA3.1-His-Ub K63-only	This Paper	N/A
pcDNA3.1-His-Ub K48-only	This Paper	N/A
pGEX-6p-3-Akt1	This Paper	N/A
pGEX-6p-3-Akt2	This Paper	N/A
pGEX-6p-3-Akt3	This Paper	N/A
pGEX-6p-3-RNF8	This Paper	N/A
TG006-RNF8	This Paper	N/A
TG006-RNF8-ΔRING	This Paper	N/A
TG006-Akt	This Paper	N/A
TG006-Akt-E17K	This Paper	N/A
TG006-Akt-K8/14R	This Paper	N/A
LentiCRISPRv2-sgRNF8-1	This Paper	N/A
LentiCRISPRv2-sgRNF8-2	This Paper	N/A
CON077 vector	GeneChem	N/A
GV112-shRNF8-1	GeneChem	N/A
GV112-shRNF8-2	GeneChem	N/A
Software and algorithms		
GraphPad Prism 5.0	GraphPad Software, USA	https://www.graphpad.com/
SPSS 17.0	IBM	https://www.ibm.com/us-en/?ar=1
Adobe Photoshop	Adobe	https://www.adobe.com/
ImageJ	Scientific Community Image Forum	https://imagej.nih.gov/ij/

RESOURCE AVAILABILITY

Lead contact

- Further information and requests for resources and reagents should be directed to and will be fulfilled by the lead contact, Genze Shao (gzshao@bjmu.edu.cn).

Materials availability

- This study did not generate new unique reagents. Plasmids generated in this study are available from the lead contact upon request.

Data and code availability

- This study did not generate any unique datasets or code. Microscopy data reported in this paper will be shared by the lead contact upon request.
- The publicly available mRNA expression and clinical information analyzed in Figures S1B, S6C, and S6D were downloaded from Oncomine, Kaplan-Meier Plotter and the Human Protein Atlas respectively. The uniform resource locators (URLs) of these databases are listed in the Key resources table.
- Any additional information required to reanalyze the data reported in this paper is available from the lead contact upon request.

EXPERIMENTAL MODEL AND SUBJECT DETAILS

Cell lines

Human embryonic kidney HEK293T, human bronchial epithelial cells 16HBE, lung cancer cell lines A549, H1299, H460 and H520 were purchased from American Type Culture Collection (ATCC) and preserved in our laboratory. H1975 was a gift from Dr. Hongying Zhen (Peking University Health Science Center). Mouse embryonic fibroblasts (MEFs) are gifts from Dr. Mo Li (Peking University Third Hospital). These cell lines have been authenticated by short tandem repeat (STR) profiling and were all grown in Dulbecco's modified Eagle's medium (DMEM) supplemented with 10% fetal bovine serum (FBS) at 37°C with 5% CO_2 in a humid atmosphere.

Mice

All mice used in the *in vivo* tumorigenesis assay were 4 weeks' male BALB/c nude mice. They were obtained from the Experimental Animal Center of Peking University Health Center (Animal Study Permit No. SYXK 2016-0010) and maintained in an environment with a standardized barrier system, which has in keeping with national standard Laboratory Animal-Requirements of Environment and Housing Facilities (GB 14925—2001). The care of laboratory animal and the animal experimental operation have conforming to Beijing Administration Rule of Laboratory Animal.

Human tissue

Lung cancer patient tissues were obtained from National Human Genetic Resources Sharing Service Platform (2005DKA31200) and The Affiliated Hospital of Qingdao University. All patients enrolled in this study have signed informed consent. Tissue sections were cut onto adhesive-coated glass slides at 3 μm thickness.

METHOD DETAILS

RT-PCR

Total RNA was isolated from cultured cells (16HBE, A549, H1299, H460, H1975 and H520) using TRIzol reagent (Thermo Fisher Scientific). Reverse transcriptions were prepared from 2 μg RNA using M5 HiPer First Strand cDNA Synthesis Kit (Mei5bio). PCR were performed using GoldenStar T6 Super PCR Mix (TSINGKE). Primers for mRNAs: RNF8 and GAPDH were as previously described in Zhu et al. (2020).

Plasmids and cloning

For construction of HA-RNF8, Flag-Akt plasmid, full-length cDNA encoding RNF8 and Akt were amplified by PCR and subcloned into pcDNA3.1 empty plasmid. RNF8 and Akt mutants were generated using site-direct mutagenesis. The amino acid sequence of the deletion of RNF8 ΔR is 403-441. For bacterial expression, N-terminal fusions to GST of Akt1, Akt2, Akt3 and RNF8 were generated by subcloning into the pGEX-6P-3 vector using BamHI and EcoRI. For generation of stable A549 and H460 RNF8 knock out cells, sgRNF8-1 and −2 were subcloned into the lentiCRISPRv2 vector. Meanwhile, Akt, AktE17K, Akt2KR, RNF8 and RNF8 ΔR were subcloned into the TG006 vector using SwaI and PacI.

Transfection of plasmids and siRNA

Plasmid transfections were performed using jetPRIME (Polyplus) according to the manufacturer's protocol. For optimal DNA transfection conditions, cells were incubated with transfection mix when they were 60%–80% confluent. Transfection medium were replaced by regular growth media 6-8 h after transfection and analyzed after 18-20 h.

siRNA transfections were also performed using jetPRIME (Polyplus) according to the manufacturer's protocol. For optimal siRNA transfection conditions, cells were incubated with transfection mix when they were 30%–50% confluent. Transfection medium were exchanged by fresh media 12-16 h after transfection and analyzed after 60-64 h.

Immunoprecipitation (IP) and immunoblotting (IB)

Cells were washed with ice-cold PBS, lysed in RIPA buffer (50 mM Tris-HCl pH 7.4, 1% NP40, 0.5% Na-deoxycholate, 0.1% SDS, 150 mM NaCl, 2 mM EDTA, and 50 mM NaF) supplemented with protease inhibitor cocktail (Sigma) and Phenylmethylsulfonyl Fluoride (Sigma), scraped and incubated in cold tubes for 30 min on ice. Cell lysates were centrifuged at 12,000 rpm at 4°C for 20 min, and supernatant was used for determining protein concentration by Bradford assay (Bio-Rad). SDS sample buffer was added to the lysates and standard immunoblotting procedures were followed. For IP, cells were lysed and quantified for protein concentration. The primary antibody was added and incubated in 4°C rotation rack overnight. Protein G beads were then added for additional 3 h at 4°C with rotation. The resin was then centrifuged for 4 min at 550 × g, washed three times with lysis buffer and analyzed by immunoblotting. Antibodies used are all listed in the Key resources table.

Immunofluorescence microscopy

Cells grown on coverslips were fixed in 4% PFA at room temperature (RT) for 10 min, permeabilized in 0.4% Triton X-100 at RT for 10 min and blocked with 10% goat serum at RT for 1 h. The coverslips were then incubated with primary antibody at 4°C overnight, followed by incubation with corresponding secondary antibodies at 37°C for 1 h. Coverslips were mounted with DAPI (Vector Laboratories). Images were collected using a Leica DM5000B fluorescence microscope.

In vivo and *in vitro* ubiquitination assay

For *in vivo* ubiquitination assay, 293T cells were transfected with the indicated plasmids for 48 h, harvested and lysed using denaturing buffer (6 M guanidine-HCl, 0.1 M Na_2HPO_4/NaH_2PO_4, 10 mM imidazole). Cell extracts were then incubated with nickel beads for 4 h, washed, and subjected to IB analysis.

For *in vitro* ubiquitination assays, recombinant GST-RNF8 and GST-Akt proteins were purified from the bacterial lysates of BL21 competent cells. Purified GST, GST-Akt and GST-RNF8 proteins were incubated for 3 h at 37°C in 30 μL of reaction buffer (20 mM

HEPES pH 7.4, 10 mM $MgCl_2$, 1 mM DTT, 59 mM ubiquitin, 50 nM E1, 850 nM of Ubc13/Uev1a, 1 mM ATP). After incubation, protein mixtures were diluted in NETEN150 buffer (150 mM NaCl, 20 mM Tris-HCl, pH 7.4, 0.1% NP-40, 0.5 mM EDTA, 1.5 mM $MgCl_2$, 10% Glycerol) and the supernatant fluid was precleared with Protein A/G beads for 1 h, followed by immunoprecipitation overnight with anti-Akt antibody, after which Protein A/G beads were added for an additional 3 h. Beads were washed four times with NETEN150 Buffer. Proteins were eluted in SDS-sample buffer and subjected to IB analysis.

Cell fractionation

Cell fractionation was performed as described in Gao et al., (2006). Briefly, cells were harvested, washed with PBS and resuspended in nuclei isolation buffer (NIB;15 mM Tris-Cl pH 7.5, 60 mM KCl, 15 mM NaCl, 5 mM $MgCl_2$, 1 mM $CaCl_2$, 1 mM DTT, 2 mM sodium vanadate, 250 mM sucrose, protease inhibitor cocktail and 1 mM PMSF). An equal volume of NIB buffer containing 0.6% NP40 was added to the cells. After centrifugation, the nuclei were pelleted, and the supernatant was recovered as a cytosolic fraction.

The cell nuclei were suspended in nuclei extraction buffer (NEB; 25 mM Tris-Cl pH 8.0, 250 mM NaCl, 1 mM EDTA, 10% glycerol, 0.2% NP40 and protease inhibitor cocktail). A total of 250 U of DNase I and 5 mM $MgCl_2$ were added to 1 mg DNA equivalent. After digestion at 4°C for 1 h, 10 mM of EDTA was added to nuclei samples. After centrifugation, the supernatant was recovered as a nuclear fraction.

Membrane fractionation

Cytosolic and membrane fractions were prepared using the Mem-PERTM Plus kit (Thermo Fisher Scientific) according to the manufacturers' standard procedures.

Apoptosis assay

A total of 5×10^5 cells were harvested, washed with ice-cold PBS and treated with the Annexin V-PE/7-AAD Apoptosis Kit (Yeasen). Briefly, 5 μL Annexin V-PE and 10 μL 7-AAD were added into 100 μL binding buffer and cells were treated with the mixed solution for 15 min in the dark at 25°C. Then the cells were analyzed with fluorescence-activated cell sorting (Beckman-Coulter, CA, USA) and the apoptotic rate was calculated.

In vivo tumorigenesis assay

5×10^6 of A549 cells with different treatments were suspended in 100 μL of PBS and then mixed with 100 μL of Matrigel (BD Biosciences) at a 1:1 ratio. Cells above were subcutaneously injected into 4 weeks' male BALB/c nude mice (n = 5). The tumor size was measured by the caliper, and the tumor volume was calculated by the equation: $[mm^3]$ = (length [mm]) × (width [mm])^2 × 1/2.

Cell growth assay

For Dox administration, 3×10^5 of WT and RNF8 KO A549 cells were seeded in 6-wells in triplicate for 24 h and treated with 2 μM Dox. 24 h later, cells were harvested, stained with trypan blue, and viable cells were counted directly under the microscope using a hemocytometer, all the experiments were repeated at least 3 times.

Immunohistochemistry and scoring

IHC staining was performed following the standard manufacturer's instruction. Briefly, after deparaffinizing and rehydrating, the slides were treated with 3% H_2O_2 solution for 15 min at room temperature to block endogenous peroxidase. The slides were then soaked in EDTA antigen retrieval buffer pH 9.0 (ZSGB-BIO) at 96°C for 20 min. After blocking using 10% goat serum, the slides were incubated with primary antibodies targeting RNF8 (Santa cruz, sc-271462) or p-AktS473 (CST, 4060) at 4°C overnight. The slides were incubated with the secondary antibody for 30 min and developed with 3,3-diaminobenzidine for 5 min. GTVisionTM+ Detection System/Mo&Rb (Genetech) was used for detection. Incubation without the primary antibody was used as a negative control. The staining was evaluated based on a combination of both the percentage and intensity of positively stained tumor cells to generate an H-score, which was calculated using the following equation: H-score = ΣPi (i + 1), where i is the intensity of the stained tumor cells (0 to 3), and Pi is the percentage of stained tumor cells for each intensity.

QUANTIFICATION AND STATISTICAL ANALYSIS

All data were derived from at least triplicates as indicated in figure legends. All the error bars used in the figures were obtained from three independent experiments as indicated in the relevant legends, and data were presented as mean ± standard deviation (SD). The significance is determined by χ^2 analysis or two-tailed Student's t Test. Statistical calculations were performed using SPSS 17.0 (IBM) and GraphPad Prism 5.0 (GraphPad Software, USA). *P*-values < 0.05 is considered statistically significant.